ARCJET TECHNOLOGY RESEARCH AND DEVELOPMENT
SECOND QUARTERLY PROGRESS REPORT
1 September 1964 through 30 November 1964

Prepared by

RESEARCH AND ADVANCED DEVELOPMENT DIVISION
AVCO CORPORATION
Wilmington, Massachusetts

RAD-SR-65-5
Contract NAS 3-5900

Prepared for

NATIONAL AERONAUTICS AND SPACE ADMINISTRATION
LEWIS RESEARCH CENTER
Cleveland, Ohio

ARCJET TECHNOLOGY RESEARCH AND DEVELOPMENT
SECOND QUARTERLY PROGRESS REPORT
1 September 1964 through 30 November 1964

Prepared by

RESEARCH AND ADVANCED DEVELOPMENT DIVISION
AVCO CORPORATION
Wilmington, Massachusetts

RAD-SR-65-5
Contract NAS 3-5900

27 December 1964

Prepared for

NATIONAL AERONAUTICS AND SPACE ADMINISTRATION
LEWIS RESEARCH CENTER
Cleveland, Ohio

ABSTRACT

This report presents the experimental and analytical data obtained from research conducted under the Arcjet Technology Development Program for the period from 1 September to 30 November 1964.

PRECEDING PAGE BLANK NOT FILMED.

CONTENTS

ILLUSTRATIONS

I. INTRODUCTION

A. PROGRAM OBJECTIVES

The objective of this program, entitled ArcJet Technology Research and Development, conducted under Contract NAS 3-5900, is to perform necessary research and development to (1) establish the upper specific impulse limit for reliable long duration operation of the radiation cooled 30-KW arcjet thrustor developed under earlier programs, (2) explore increases in specific impulse and efficiency which appear to be associated with operation at lower propellant mass flow rates with and without external magnetic fields, and (3) characterize the performance of the arcjet engine operated in a pulsed mode.

B. PROGRAM ORGANIZATION

This program originates from the Electric Propulsion Office of the NASA Lewis Research Center. Mr. Henry Hunczak is Project Manager for the Electric Propulsion Office. Dr. R. R. John is Project Director at Avco RAD, and Dr. S. Bennett is Associate Project Director. Mr. J. F. Connors is Project Engineer. Principal Avco RAD participants and the areas in which they contribute are: Drs. A. Tuchman, and M. Clark, Thrustor Diagnostics and Performance Analysis; J. Connors, Thrustor Life Tests; G. Enos and C. Simard, Thrustor Performance Testing.

C. PROGRAM SCHEDULING

This is the second quarterly progress report submitted under Contract NAS 3-5900; it covers the period from 1 September to 30 November 1964. Data on contract costs and manpower expenditures have been submitted previously in the monthly progress reports dated 10 October 1964 (4), 10 November 1964 (5), and 10 December 1964 (6).

D. TECHNICAL SUMMARY

During the second quarter, primary attention, both experimental and analytical, was directed toward item (2) listed among the program objectives. In particular, propulsion performance data was obtained with hydrogen and ammonia as propellants over a wide range of propellant flow rates, arc currents, arc powers, and applied magnetic field strengths. Overall efficiency values (at input power levels of 20 to 160 kw) for hydrogen were 25 percent at 3000 seconds, 30 percent at 4000 seconds, and 40 percent at 5000 seconds; for ammonia, (at input power levels of 20 to 80 kw) 30 percent at 3000 seconds, 35 percent at 3500 seconds. Data were also obtained with helium, argon, and nitrogen as propellants. An effort has been made to separate the contributions to the experimentally measured thrusts from the different thrust producing mechanisms. In this way an estimate has been made of the Hall component of thrust, T_{Hall}, which has been found to be

a linear function of the product of the applied magnetic field strength, B, and the arc current, I.

In the portion of the program dealing with the 30-kw radiation cooled engine, an unsatisfactory braze was obtained with the 75 percent W-25 percent Re engine, and the long duration test has consequently been rescheduled.

II. MPD ARCJET ENGINE

A. INTRODUCTION

While arcjet engines and Hall accelerators have been under development at a number of laboratories[1,2,3] over the past five years, only within the past year has the specific impulse level of 2,500 seconds been exceeded. The acceleration mechanisms which produce the greatly increased specific impulse levels now attainable appear to be a combination of aerodynamic, self-magnetic, and applied magnetic field effects. These mechanisms, in different proportions, are now being used in the different laboratories to achieve specific impulse values from 2,500 to 10,000 seconds, with major effort concentrated in the 3,000 to 5,000 second range. A basic geometry, illustrated in figure 1, characterizes virtually all of the improved accelerators. The units are cylindrically symmetrical, consisting of a central cathode surrounded by a coaxial anode. A magnetic coil is mounted coaxially with the thrustor, with the thrustor exit plane generally slightly downstream of the downstream edge of the coil.

Reference 4 discusses in some detail five basic thrust-producing mechanisms which have been identified in the literature as being characteristic of plasma generators of the type illustrated in figure 1. These are (1) aerodynamic pressure forces; (2) magnetic pumping; (3) magnetic blowing; (4) aerodynamic swirl induced by MPD forces; and, (5) Hall current acceleration.

Defining the thrust resulting from mechanism (1) as T_{aero} and the thrust from mechanisms (2) and (3) as T_{Self} it is shown in reference 4 that

$$T_{aero} \sim P_c A_t \tag{1}$$

and

$$T_{Self} = T_{pump} + T_{blow} \tag{2}$$

where
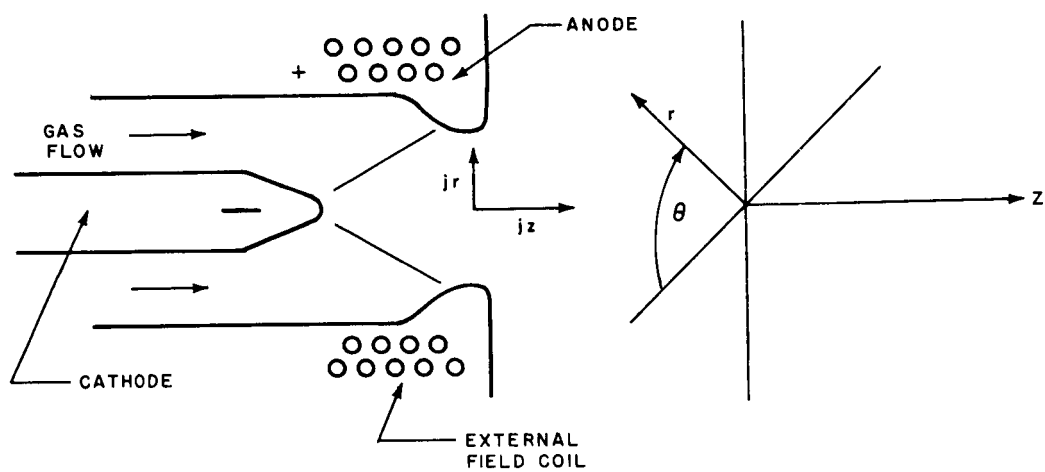
$$T_{pump} = 5.1 \times 10^{-6} I^2 \tag{3}$$

and

$$T_{blow} = 1.02 \times 10^{-5} I^2 \left(1/4 + \ln \frac{r_a}{r_c} \right) \tag{4}$$

when the current enters the cathode uniformly after leaving the anode as a ring, or

$$T_{blow} = 1.02 \times 10^{-5} I^2 \left(\ln \frac{r_a}{r_c} \right) \tag{5}$$

-3-

Figure 1 SCHEMATIC OF HIGH SPECIFIC IMPULSE ACCELERATOR

64-10326

when the current distribution at the cathode is similar to the distribution at the anode.

In equations (1) through (5),

T_{aero} = aerodynamic thrust component, grams

P_c = chamber pressure, grams-force/cm^2

A_t = throat area, cm^2

T_{Self} = Self MPD thrust, grams

T_{pump} = magnetic pumping thrust, grams

T_{blow} = magnetic blowing thrust, grams

I = arc current, amperes

r_a = outer radius of current distribution at anode, cm

r_c = outer radius of current distribution at cathode, cm.

T_{pump} results from the interaction of the axial discharge current density, j_z, with the self-induced magnetic field, B_θ. T_{blow} results from the interaction of the radial discharge current, j_r, with the self-induced magnetic field, B_θ. Both T_{pump} and T_{blow} were identified by Maecker. [5]

The magnetic swirl mechanism, (4), is associated with the bulk rotation of the gas and results from the interaction of the radial component of the current, j_r, with an axial component of the applied magnetic field, B_z, and from the interaction of j_z with B_r. In order to produce useful thrust, the rotational energy must be converted into axially directed kinetic energy by means of a nozzle. This basic thrust mechanism has been described by, among others, Hess, [6] Ellis, [8] and Powers and Patrick. [9]

Finally, the fifth thrust mechanism results from the interaction of an induced azimuthal Hall current, j_θ, with the applied magnetic field. The most likely thrust-producing interaction is the body force given by $j_\theta B_r$, but it is also possible to achieve thrust from the pressure produced by $j_\theta B_z$. These mechanisms have been investigated by Hess, [7] Seikel and Reshotko, [10] Cann, [11,12] Patrick and Powers, [13] and Gourdine. [14]

Reference 4 reports work performed at this laboratory with a plasma accelerator making use of mechanisms (1), (2), and (3). During this second quarter, mechanism (5) has been explored, and the results are presented in the following paragraphs.

B. MPD ARCJET DEVELOPMENT

1. Engine Configuration

The basic engine design used for the experimental investigations is the same as that reported in reference 4, which also presents photographs. The MPD arcjet schematic (X-2C) is given as figure 2. The central cathode consists of a thoriated tungsten tip soldered to a water-cooled copper holder. Separate coolant flows are maintained for the anode and the cathode. Propellant is injected tangentially through four ports aligned normally to the engine axis. Chamber pressure is monitored with a tap indicated in figure 2.

2. Test Systems

a. Environmental Tank

The X-2C MPD arcjet is tested in a 4-foot diameter aluminum environmental tank which is water cooled to allow for prolonged operation. The tank is 6-feet long and has two viewing ports on each side. The amount of magnetic material (such as steel fittings, hinges, etc.) within and in the immediate vicinity of the tank has been reduced to an absolute minimum. The thrust stand and its associated components are of either aluminum or nonmagnetic stainless steel. Only a portion of the heat exchanger, 6 feet from the engine, is of magnetic material producing a small tare in the thrust measurement.

A 6,000 CFM capacity mechanical pumping system is used as the primary system to evacuate the test tank. An auxilliary 34,000 CFM capacity pumping system may be used in parallel with this system. The primary system alone presently maintains the ambient tank pressure below a pressure level of 0.5 mm Hg for all mass-flow conditions. Until very recently, no major effort had been expended in order to reduce the back pressure below this level, since no extreme changes in engine performance have been noted for variations in back pressure above and below this level. Efforts have now been completed to reduce the back pressure to a level of 50-150 microns during engine operation, with a blankoff pressure of five microns. Another complete set of data points will now be obtained to determine which changes, if any, are due specifically to the reduction of ambient pressure. Several operating points have been checked so far, revealing no change with pressure level. The planned operation of one or more X-2 engines at the NASA LRC, in conjunction with the data gathered here at the 50-150-micron level, could yield a useful estimate of the engine characteristics in a hard vacuum.

INSULATOR

WATER OUT

WATER IN

GAS IN

COPPER NOZZLE

NOZZLE RETAINER RING

WATER DIVIDER

HOUSING

BORON NITRIDE SPACER

CHAMBER PRESSURE TAP

TUNGSTEN TIPPED CATHODE

CATHODE HOLDER

CATHODE GUIDE
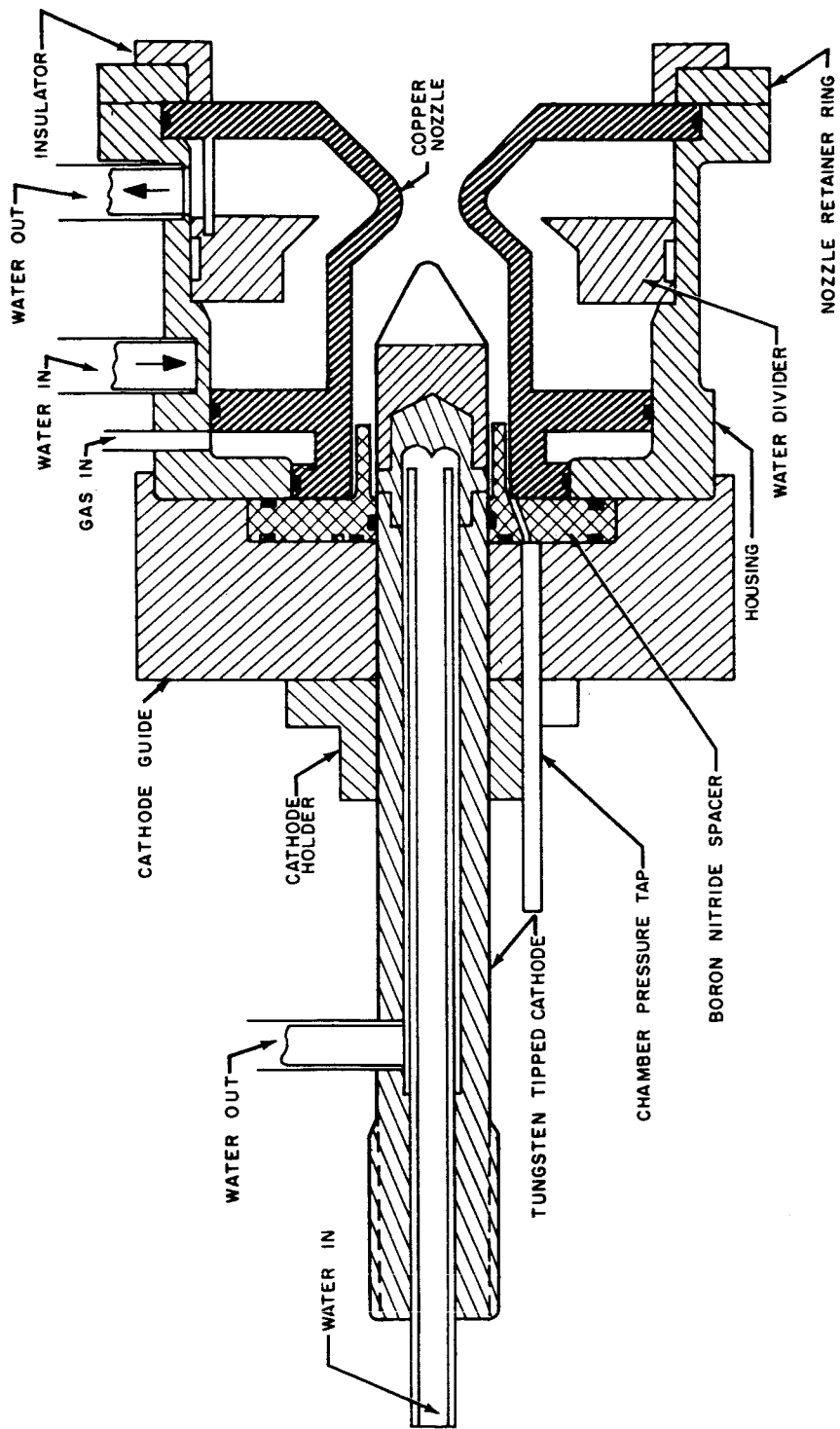
WATER OUT

WATER IN

Figure 2   HIGH IMPULSE ARCJET

64-9082

-7-

b. Magnetic Field Coil

A magnetic field coil is wound around the body of the engine with its axis coincident with the axis of the engine. The coil has an inner diameter of 7 inches, an outer diameter of 17 inches, and is 1-3/4 inches long. It consists of 40 turns of 3/8-inch OD copper tubing and is water cooled. The center of the coil is adjusted to coincide with the cathode tip. The maximum axial magnetic field strength at the center of the coil is limited to about 3 kilogauss at a current of 1800 amperes by the heat generated in the coil. The magnetic field strength is linearly dependent upon the current.

Figure 3 shows a mapping of the magnetic field. Each arrow represents a measured value of magnetic field strength. Its length is proportional to the field strength, and its direction is along the field at the point. The measured values have been used as guides to sketch in the field lines - shown as dashes in figure 3. The coil has been run at currents from 300 to 1, 200 amperes, corresponding to an axial magnetic field strength in the range 0. 5 to 2. 0 kilogauss.

c. Instrumentation

The various test and measurement equipments which are used to determine the performance characteristics of the X-2 engine are: 1) the thrust stand, 2) temperature measuring thermocouples, 3) current, voltage and mass flow meters, and 4) pressure gages. These are more fully described below.

1) Thrust stand

The engine is suspended from a thrust stand which measures thrust force directly. The thrust-stand displacement is sensed by a linear differential transformer whose output is recorded on a Sanborn type 1500 recorder. Calibration of the thrust stand in units of force is accomplished by standard pulley and weight techniques. The calibration is performed statically with the engine off, as well as during engine operation and at all operating values of magnet coil current. The thrust level is generally recorded using a sensitivity of approximately 9 gm/mm on the recorder chart for thrusts in the range from 90-200 gm, and with a correspondingly greater sensitivity for lower thrust levels.

2) Thermocouples

In order to accurately determine the thermal efficiency of the X-2 engines, the power dissipated in heating of the anode and cathode are measured by a standard calorimetric method. The temperature

-8-

COIL

X2-C ANODE

LENGTH = 1000 GAUSS

COIL CURRENT
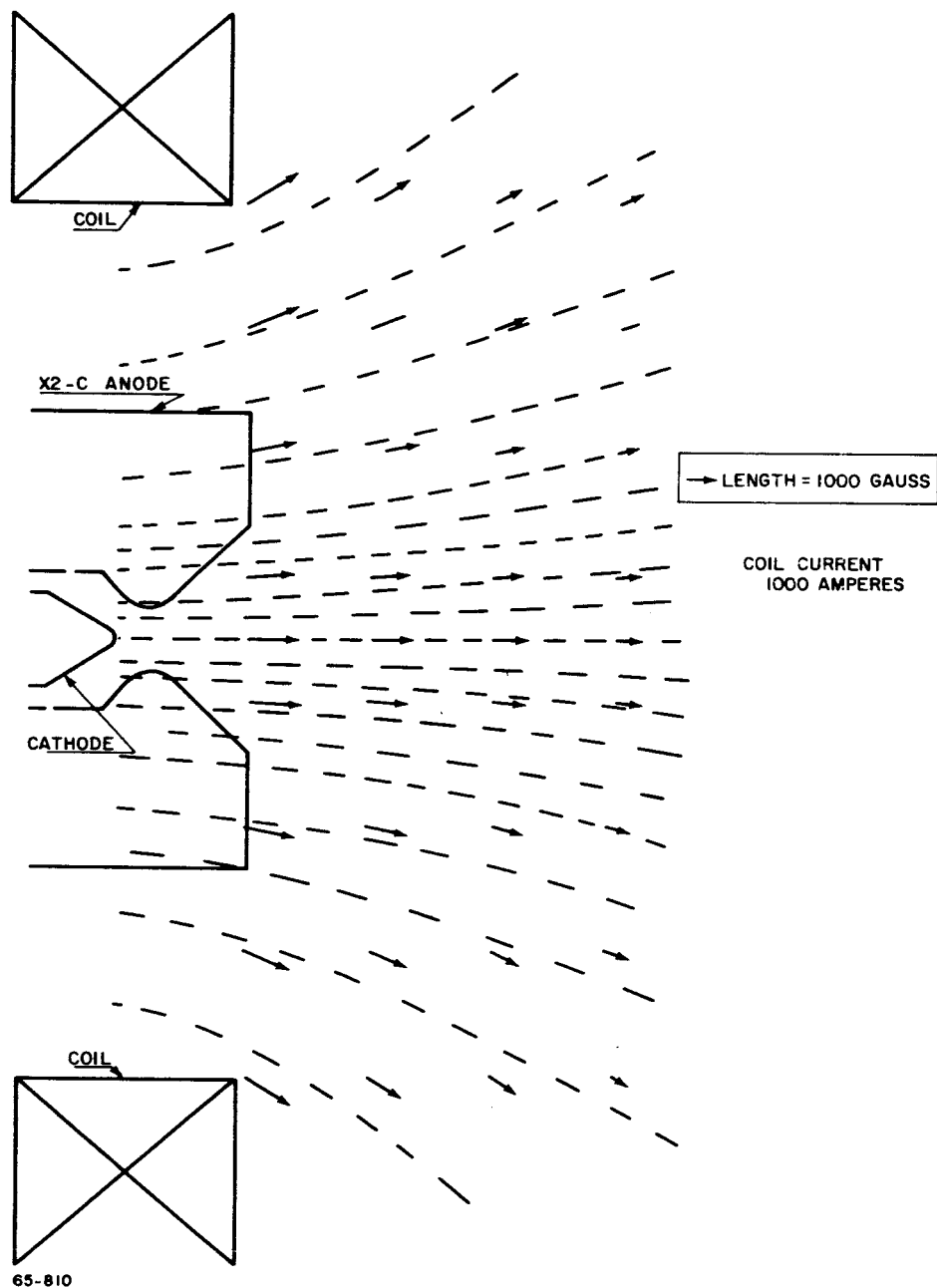1000 AMPERES

CATHODE

COIL

65-810

Figure 3 MAGNETIC FIELD MAP

rise of cooling water in the anode and cathode is measured by differential Iron-Constantan thermocouples and recorded, individually, on a Sanborn recorder. The temperature difference between water inlet and outlet is converted to heat power from a knowledge of the rate-of-water flow through the electrodes.

3) Current, voltage, and mass flow

Both arc current and coil current are measured using precision 50-mv shunt resistors and precision dc millivoltmeters. The arc voltage is measured with a precision dc voltmeter. The arc current and arc voltage are also measured and recorded on the Sanborn recorder to allow direct comparison with thrust and anode-cathode power at any time. As an extra precaution, the meter readings are hand recorded as well.

The propellant mass flow is measured with Fisher-Porter rotameter type flowmeters. Coolant flow rates are measured using standard liquid flowmeters.

4) Pressure gages

Both engine chamber pressure and ambient tank pressure are measured with precision Wallace and Tiernan vacuum gages. The chamber pressure is measured with a 0-50-mm Hg gage in parallel with a 0-800-mm Hg gage for use at high mass flows. The vent pressure gage has a range from 0-20 mm Hg. Tank pressures below about 1 mm Hg are measured with a Stokes' McLeod gage or an NRC alphatron gage.

3. Voltage - Current Characteristics

An investigation has been made of the voltage - current characteristics of the X-2C MPD arcjet operated in hydrogen and in ammonia. The variables were arc current, applied magnetic field strength, and propellant flow rate. For all of these tests the ambient tank pressure was in the range 200 to 500 microns. Power was supplied to the engine from a silicon diode rectifier with a 300-kw capability.

Figure 4 shows, for hydrogen mass flow rates of 0.02 and 0.05 gm/sec, the measured X-2C voltage as a function of arc current. The magnetic field strength is 1000 or 2000 gauss. (The magnetic field is characterized for discussion by the maximum value of the axial component, which is found at the cathode tip). In the current range shown, the voltage-current slopes are near zero. There is some experimental evidence that at lower current values the slopes are negative. At a given current in the range 500-1,600 amperes the voltage level increases with magnetic field strength and mass flow rate.
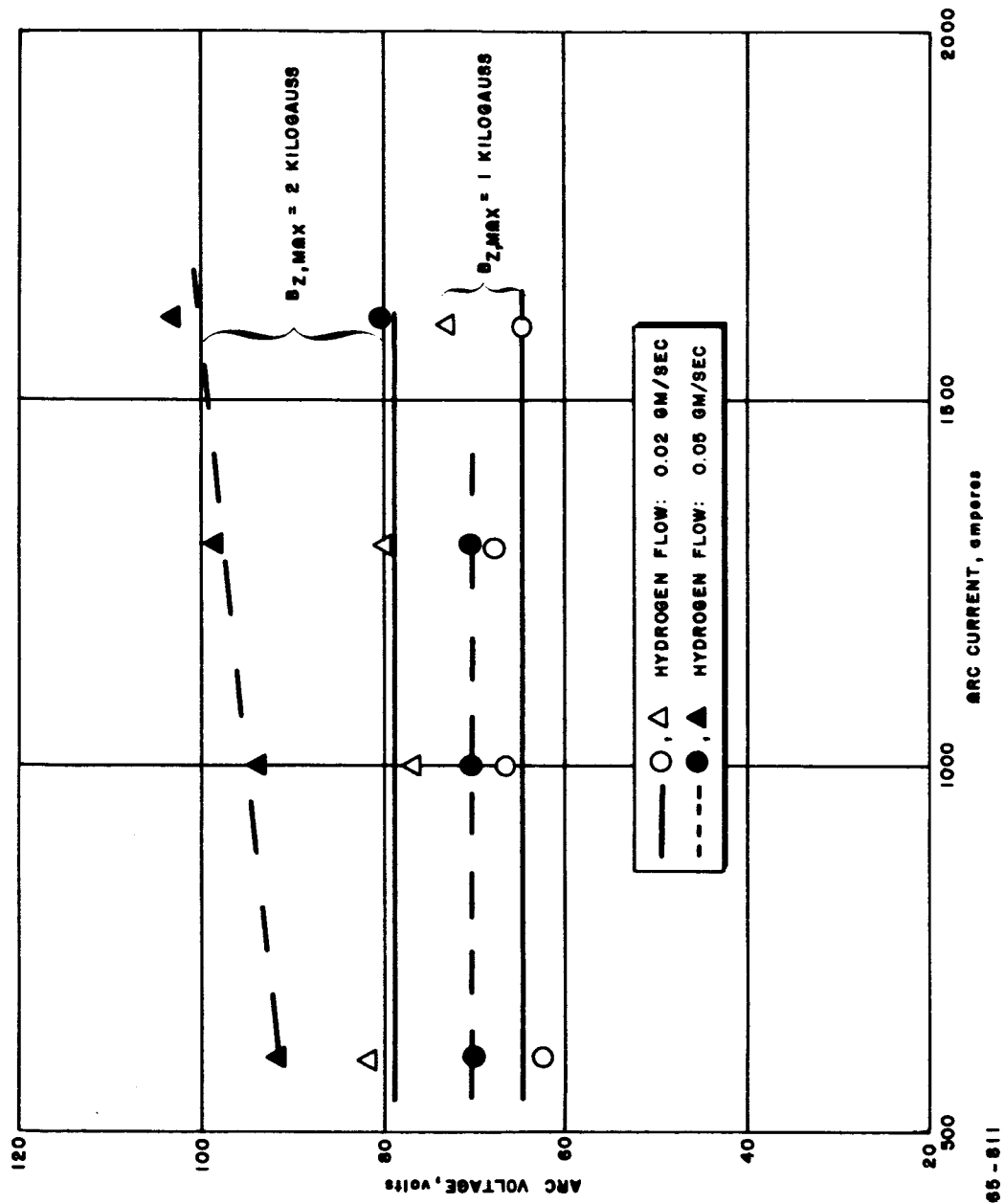
Figure 4 ARC VOLTAGE VERSUS ARC CURRENT (HYDROGEN)

65-611

-11-

Figure 5 is a plot of the voltage-current characteristics for ammonia at mass flow rates of 0.029 and 0.058 gm/sec, again for magnetic field strengths of 1,000 and 2,000 gauss. Compared with the data for hydrogen, the ammonia voltages are significantly lower; however, they show the same general lack of sensitivity of the voltage to current level, and the same tendency for voltage to increase with magnetic field and mass flow rate at a given current.

For all of the hydrogen data summarized in figure 4, the voltage spread is approximately 80 ± 20 volts. For the ammonia data of figure 5 the spread is in the range 46 ± 8 volts, so that not only is the voltage generally lower in ammonia, but the sensitivity of the voltage to variation of mass flow rate and magnetic field is also lower.

In figure 6 voltage is plotted against magnetic field strength for both hydrogen and ammonia. Data are combined for different mass flow rates and currents, contributing to the scatter in the figure. There appears, however, to be a tendency with both propellants for the voltage to rise with magnetic field strength at a rate sufficient to be apparent even with the experimental scatter.

The data of figure 6 can be fit by relations of the form

$$V = V_0 + k B \tag{6}$$

where V_0 and k are unknown constants. V is the measured voltage and B the applied magnetic field strength.

Patrick and Schneiderman,[15] have proposed a theoretical justification for a relation of this form. Paraphrasing the discussion of reference 15, it is suggested that the voltage for the device is established in that geometrical region where the initial ionization occurs. By equating the ratio E/B in this region to the critical velocity for the propellant, u_c , the relation

$$V = V_0 + u_c B \ell \tag{7}$$

is obtained, where u_c is the critical velocity (that velocity for a molecule at which the kinetic energy, $1/2 \, mv^2$, is equal to the energy required to dissociate the molecule and ionize the constituent atoms to the first level), and ℓ is an unknown length related to some geometrical feature of the plasma generator. Data obtained with hydrogen, argon, and nitrogen were correlated with this formula in reference 15, with V_0 selected for each propellant, but with a constant value of ℓ , the length. In the plasma generator of Patrick and Schneiderman, this length was taken as one centimeter, which is characteristic of the radial separation of the discharge region of attachment at the anode from the cathode tip.

$B_{Z,MAX}$ = I KILOGAUSS

○ ●

$B_{Z,MAX}$ = 2 KILOGAUSS

△ AMMONIA FLOW: 0.029 GM/SEC

▲ AMMONIA FLOW: 0.058 GM/SEC

ARC VOLTAGE, volts

100

80

60

40

20

0

500   1000   ARC CURRENT, amperes   1500   2000
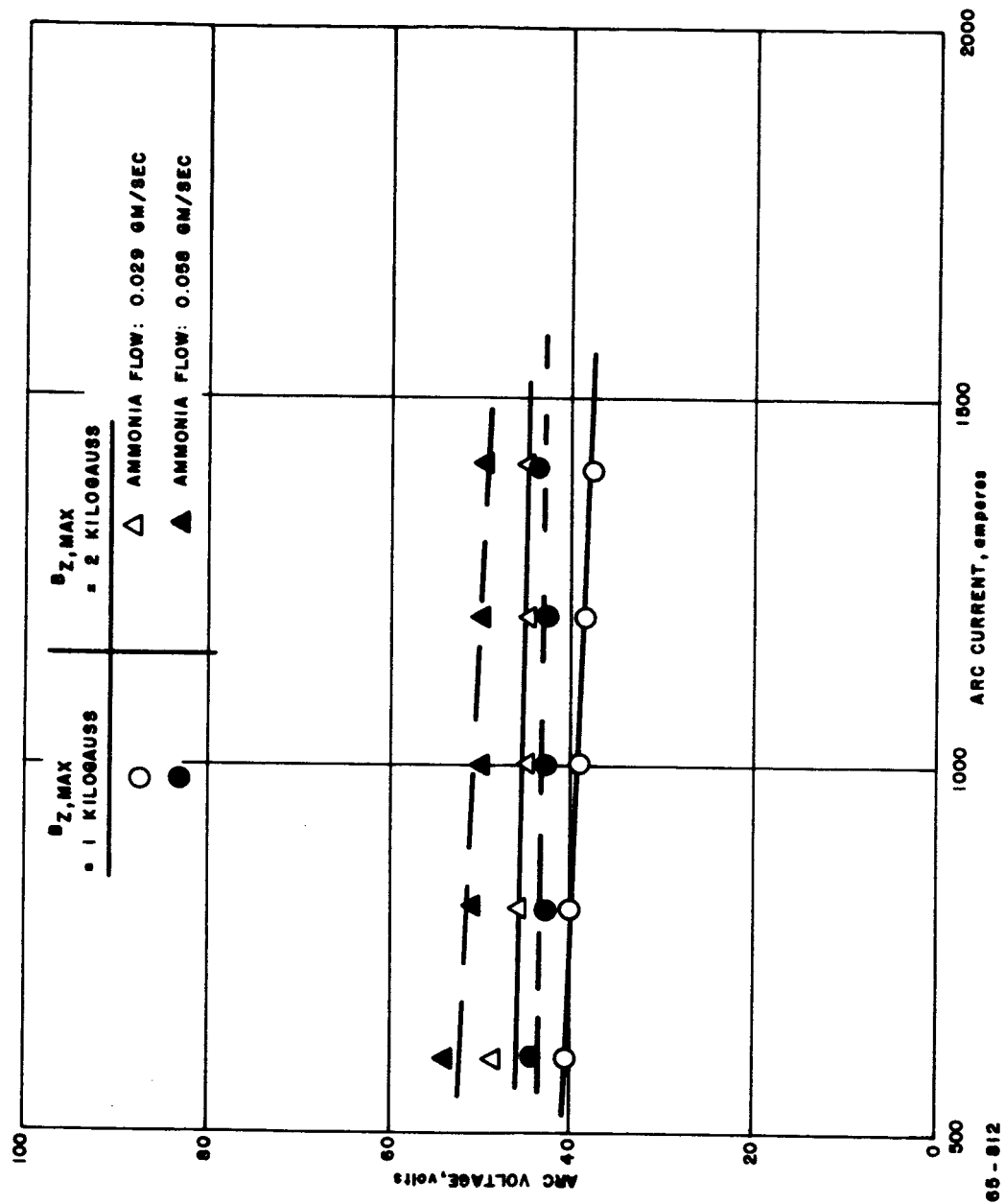
65-812

Figure 5 ARC VOLTAGE VERSUS ARC CURRENT (AMMONIA)

-13-
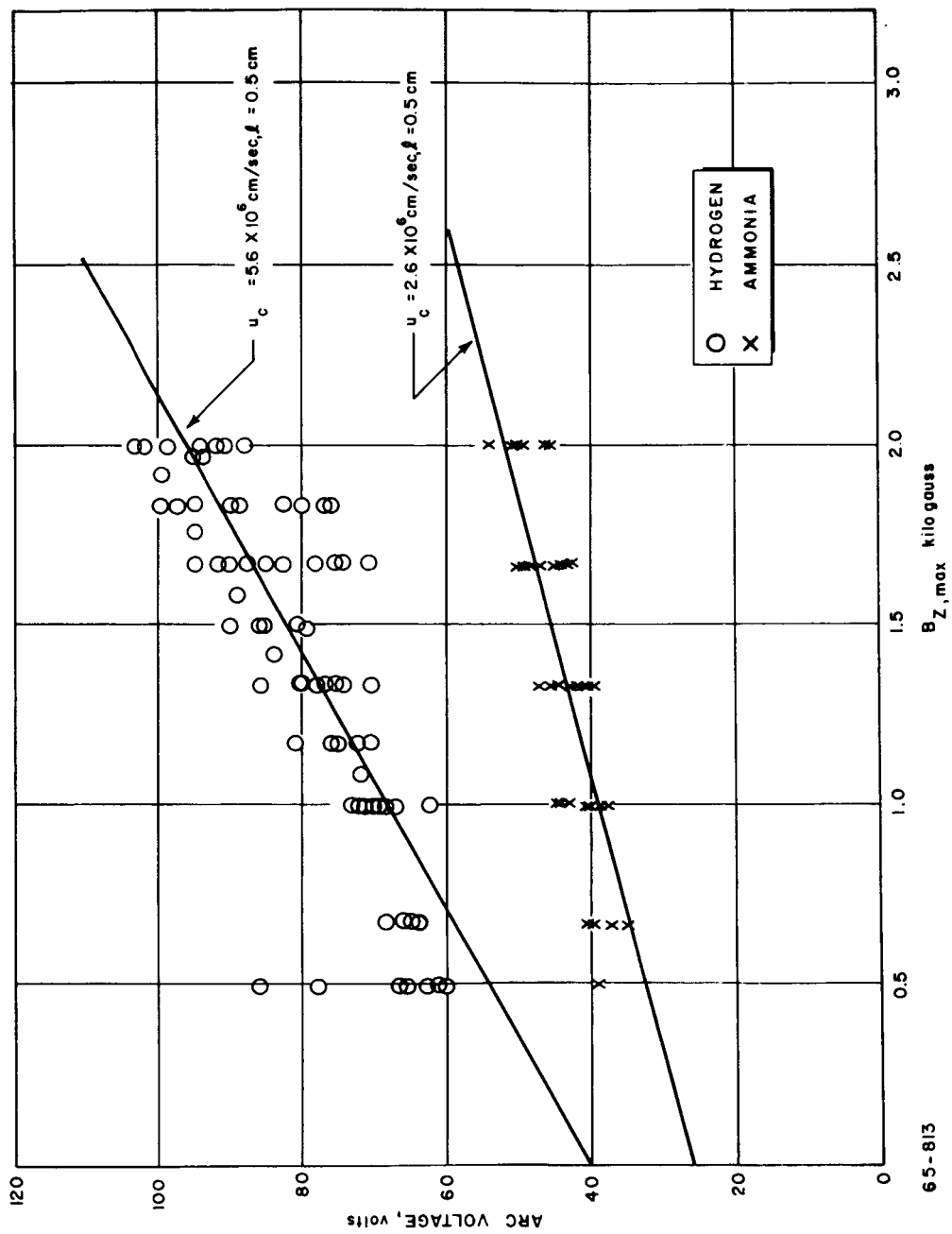
Figure 6 ARC VOLTAGE VERSUS MAGNETIC FIELD STRENGTH (HYDROGEN, AMMONIA)

65-813

-14-

The critical velocity, u_c, is 5.6×10^4 m/sec for hydrogen and 2.6×10^4 m/sec for ammonia. Selection of $V_o = 40$ volts for hydrogen, to agree with reference 15, led to a choice of $\ell = 5$ mm to fit the hydrogen data; the line drawn through the hydrogen data in figure 6 corresponds to this choice for ℓ. Keeping ℓ fixed at 5 mm, the slope for the ammonia data is fixed, and the best-fit line of this slope is drawn on figure 6.

Inspection of the fit obtainable in this way, especially for the ammonia data, indicates that agreement with the first order theory is less satisfactory for these data than for those of reference 15; however, the theory does predict a lower slope for ammonia, which is observed, and, further, it is plausible that the value of ℓ applicable to the X-2C MPD arcjet should be smaller than that reported in reference 15, since the geometry employed there is more open, while the X-2C MPD arcjet geometry employs a throat downstream of the cathode. Hence, it is quite possible that the theory is an acceptable first-order characterization of variation of voltage with magnetic field in axisymmetric MPD arcjet devices.

4. Thermal Efficiency

In this section, data are presented which determine the "thermal" efficiency of the X-2C MPD arcjet. By thermal or arc efficiency is meant the quantity

$$\epsilon_{arc} = \frac{\text{Power to gas}}{\text{Power to arc}} \tag{8}$$

where the power input is taken as the product of applied voltage and arc current without correction for the incoming gas enthalpy. For the enthalpy levels associated with the X-2C MPD arcjet this correction is negligible. (Actually, much of the power input to the engine is in the form of directed kinetic energy without passing through a thermal stage, but the term "thermal efficiency" is taken over from the usual arc heater terminology). The heater efficiency is determined by measuring the power lost to the anode and cathode water cooling circuits, according to equation 9

$$\epsilon_{arc} = 1 - \frac{P_{cool}}{P_{in}} = 1 - \frac{\dot{m}_w \, c_{p,\,w} \, \Delta T_w}{VI} \tag{9}$$

where $\dot{m}_w$, $c_{p,\,w}$, and ΔT_w are the mass flow rate, specific heat, and temperature rise, respectively, of the coolant water.

In practice, the cathode heat loss is small under all conditions of X-2C MPD arcjet operation, varying between approximately 0.5 and 2 kilowatts as a function of current and mass flow rate. The anode heat loss, on the other hand, is in general, substantial.

-15-

In figure 7 P_{cool} in kilowatts is plotted as a function of current for a number of test runs of the X-2C MPD arcjet. The tests were made in hydrogen at mass flow rates of 0.02 and 0.05 gm/sec, and with applied magnetic field strengths varying from 500 to 2,000 gauss. Data points corresponding to the mass flow rate of 0.02 gm/sec are indicated by open circles, while those for the 0.05 gm/sec flow rate are represented by crosses. In addition to these points are plotted several reported by Cann[16] and by Ducati[17]; the data of reference 16 were obtained at a hydrogen flow rate of 0.02 gm/sec, while those of reference 17 correspond to a hydrogen flow rate of 0.025 gm/sec.

Several features are clear from inspection of figure 7. First, the correlation of P_{cool} with current is fairly good; the data points corresponding to different mass flow rates and to different magnetic field strengths exhibit relatively little scatter. Second, the data reported by Cann[16] and by Ducati[17] also correlate reasonably well with those measured at this laboratory, although there are differences in the MPD arcjet geometry and magnetic field configuration among the devices employed at the three laboratories. Finally, these data can be represented reasonably well over most of the current range by a straight line of slope equal to unity, which is consistent with a constant voltage drop at the electrodes representing most of the heating. At the highest currents P_{cool} tends to fall away from this line, but within about 30 percent the data for currents ranging from 100 to 3000 amperes can be accounted for by a constant voltage drop of about 26 volts. In contrast, the sensitivity of the anode and cathode heat transfer to mass flow rate seems very slight.

The line drawn on figure 7 is simply a smooth curve fitted by inspection to the data. This same smooth curve is repeated on figure 8, where P_{cool} is plotted as a function of current for X-2C operation with ammonia as the propellant. The ammonia mass flow rates represented in figure 8 are 0.029 and 0.058 gm/sec compared with the hydrogen flow rates of 0.02 and 0.05 gm/sec of figure 7. The magnetic field variation for the data of figure 8 is again 500 to 2000 gauss. Inspection of figure 8 reveals that the data are fitted remarkably well by the line drawn to represent the hydrogen data of figure 7; therefore, the major features of the electrode heating in hydrogen operation are applicable also to operation in ammonia. Again, sensitivity to mass flow rate of propellant is slight for the two mass flow rates plotted in figure 8.

The success in fitting heat transfer data for both hydrogen and ammonia with a single curve motivates examination of data which have been obtained in other gases as well. Figures 9, 10, and 11 are curves analogous to figures 7 and 8, and are drawn for helium, nitrogen, and argon. In each case the smooth curve is the one which was fitted to the hydrogen data of figure 7.
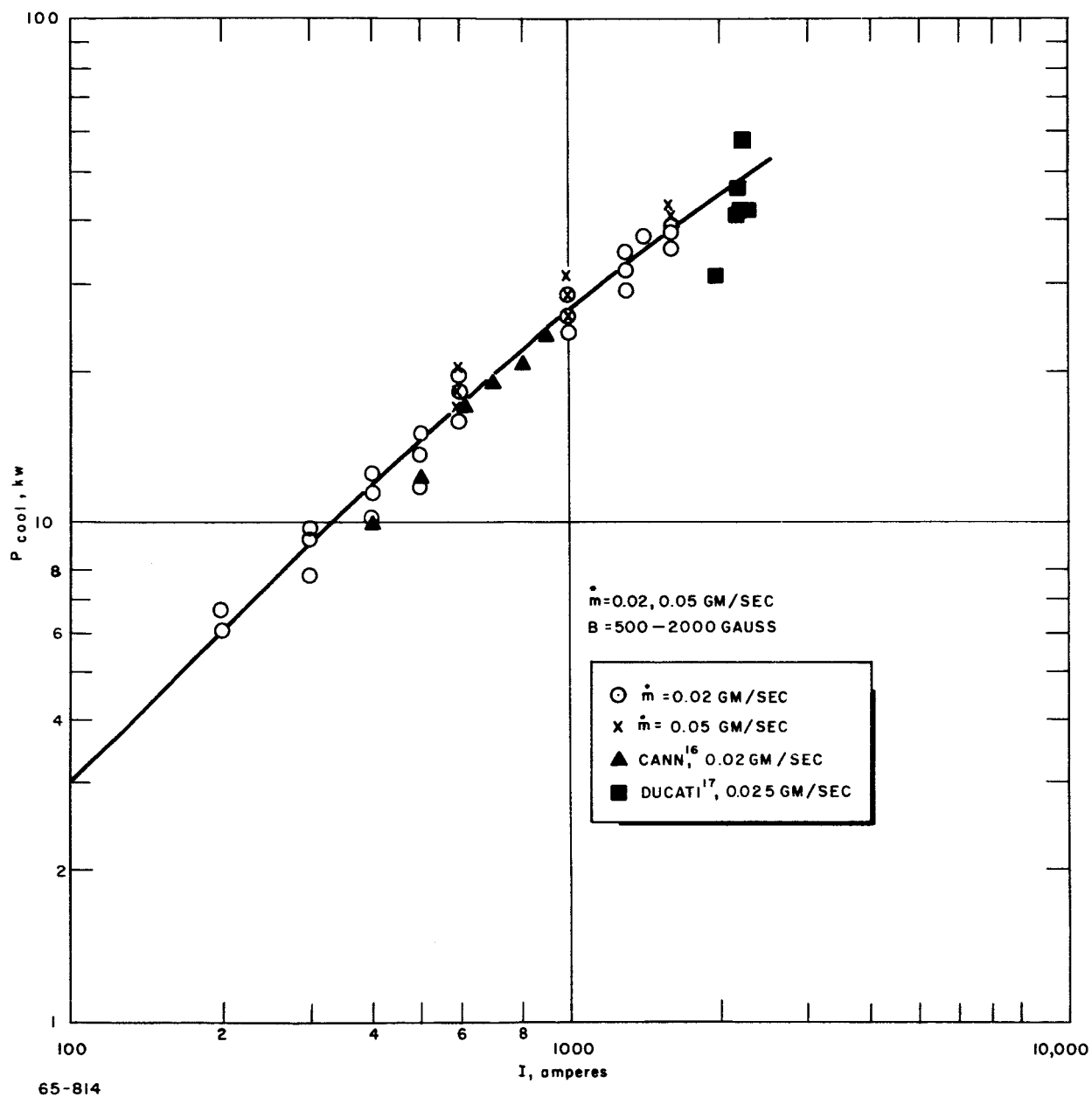
Figure 7 POWER TO COOLING VERSUS ARC CURRENT (HYDROGEN)

65-814

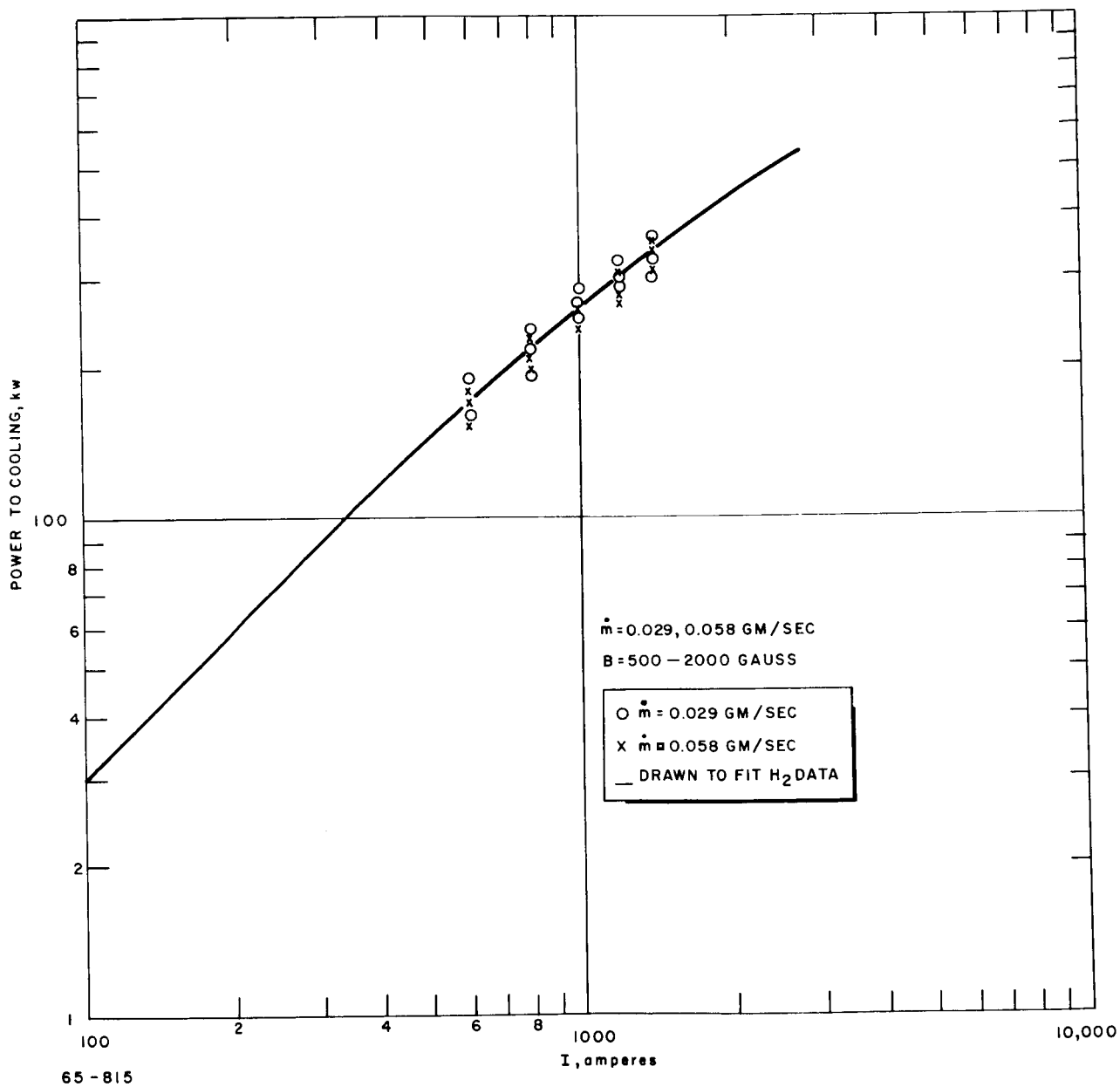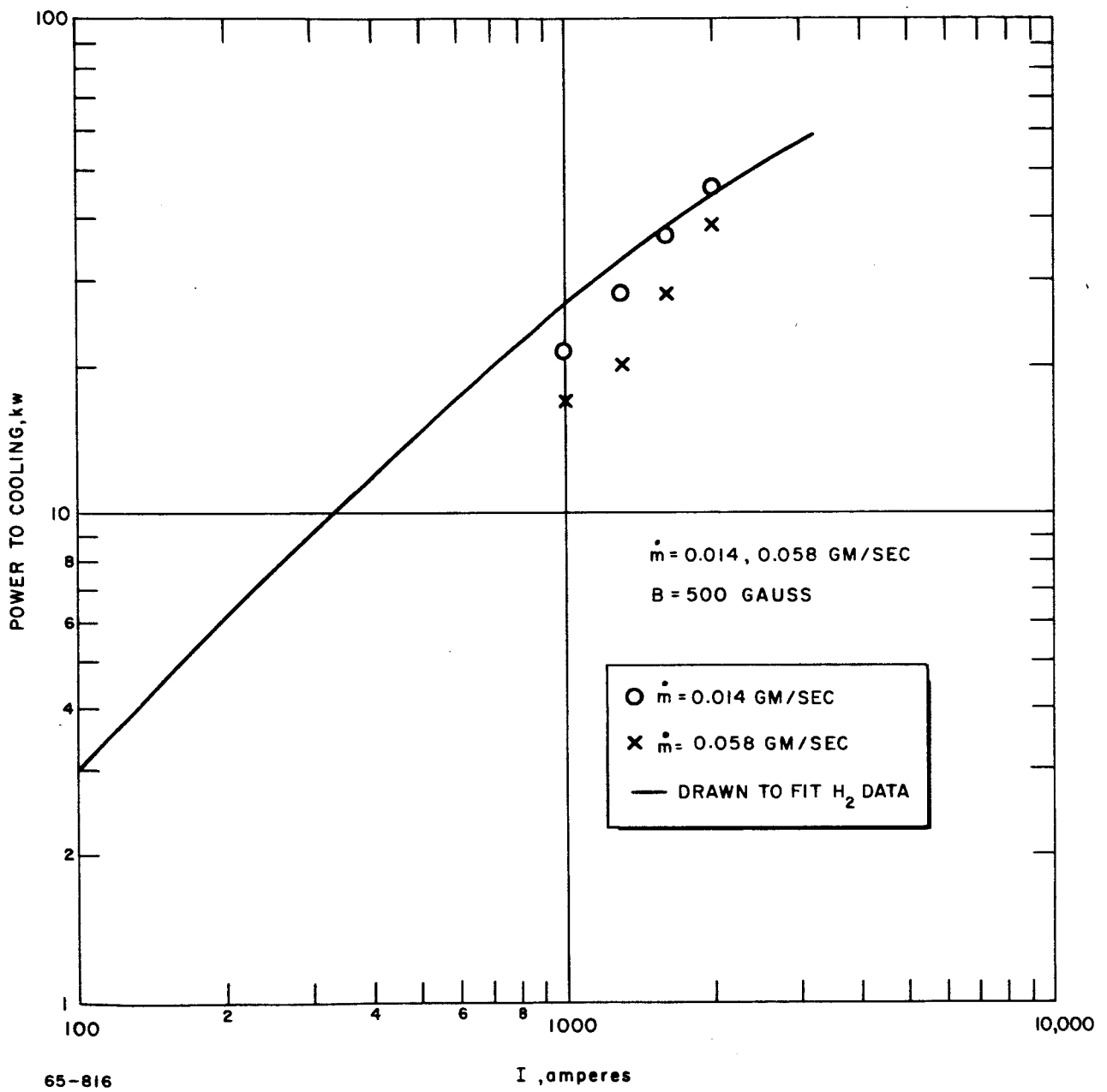Figure 8 POWER TO COOLING VERSUS ARC CURRENT (AMMONIA)

65 - 815

-18-

Figure 9 POWER TO COOLING VERSUS ARC CURRENT (HELIUM)
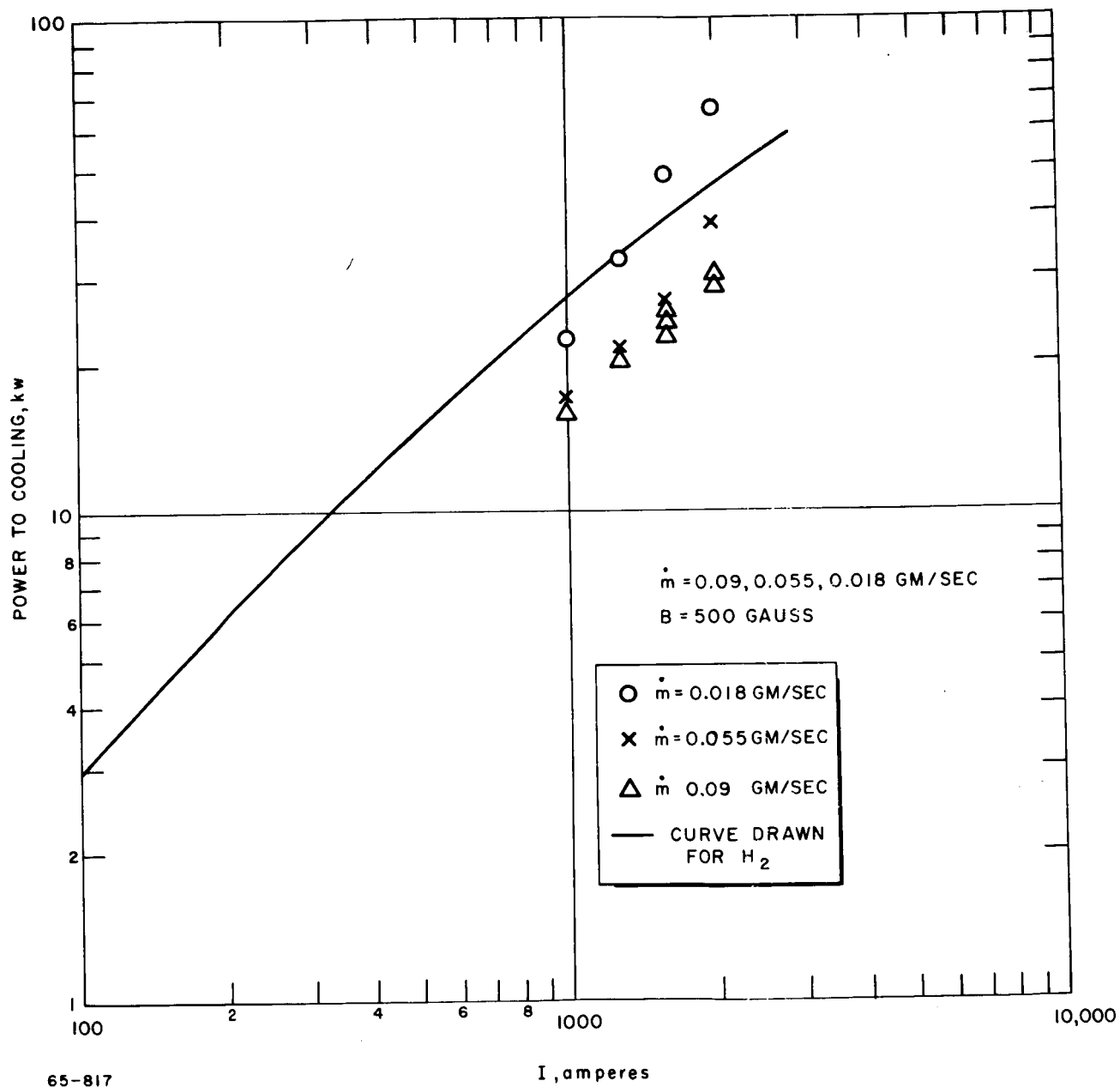
65-816

Figure 10 POWER TO COOLING VERSUS ARC CURRENT (NITROGEN)

-20-
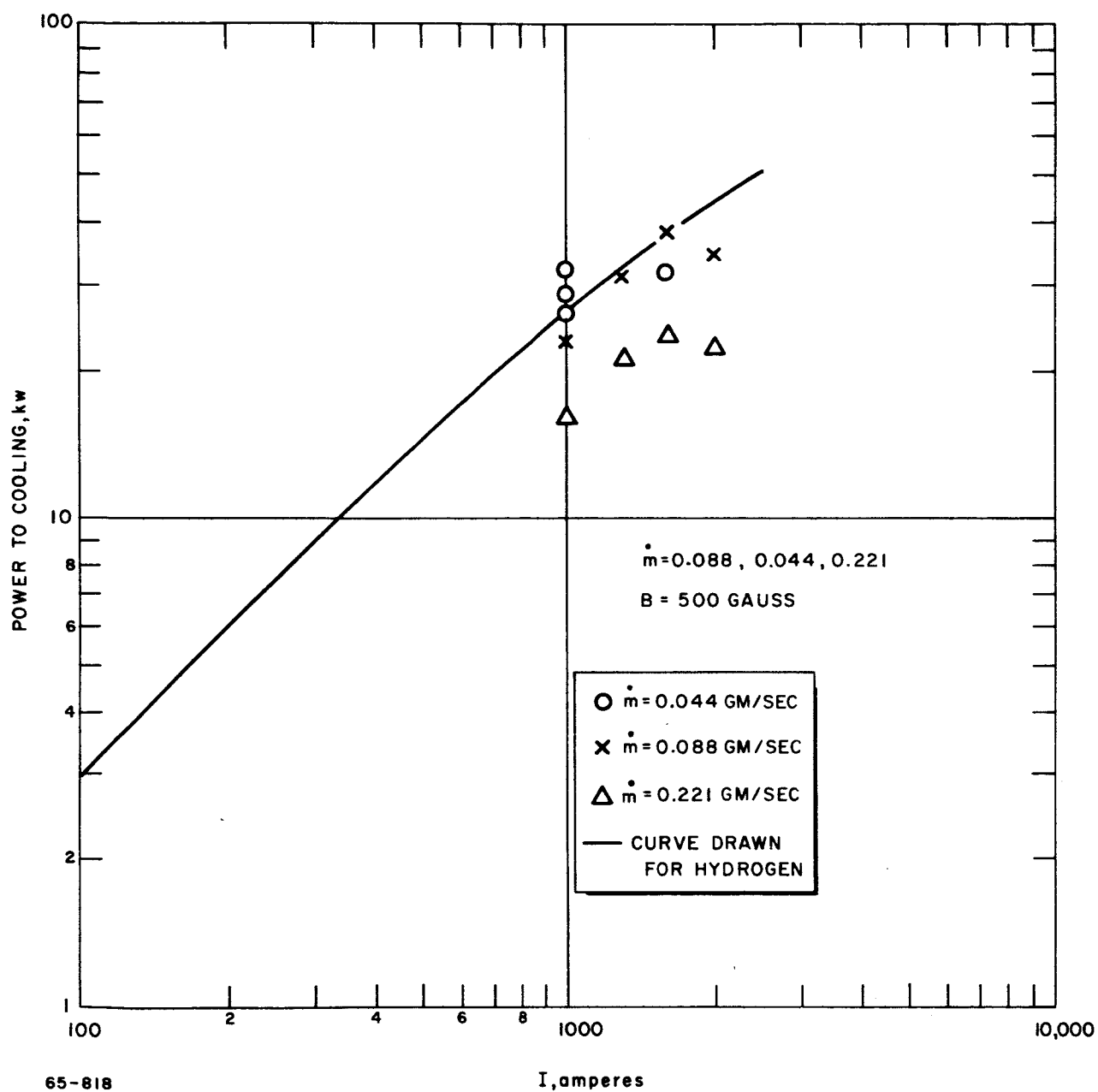
Figure 11 POWER TO COOLING VERSUS ARC CURRENT (ARGON)

65-818

-21-

In figure 9, data are presented for helium mass flows of 0.014 and 0.058 gm/sec; only a single magnetic field strength of 500 gauss was employed. The scatter of these few data points is more severe, and it is not at all certain that the quantitative trend of P_{cool} with current is precisely the same as for hydrogen; further there appears to be a systematic but small dependence upon mass flow rate. Still, the hydrogen curve fits the data tolerably within the accuracy with which the helium trend can be estimated.

Figure 10, for nitrogen, can be commented upon in much the same way. There is some apparent dependence upon mass flow rate between flow rates of 0.018 and 0.055 gm/sec, but very little difference between 0.055 and 0.09 gm/sec. For the few data points which are available, the hydrogen curve provides a tolerable fit.

Finally, argon also seems to fit this general heat transfer characteristic, as indicated by figure 11. For argon there is little systematic dependence of heat transfer on mass flow rate between 0.044 and 0.088 gm/sec, but there is some effect apparently between these flow rates and 0.221 gm/sec. The hydrogen curve is again a tolerable fit.

Several conclusions may be tentatively reached on the basis of the data of figures 7 through 11. These are:

    a.   Electrode heat transfer rates are most sensitive to current among the parameters which have been varied.

    b.   Electrode heat transfer is much less sensitive to accelerator configuration (e.g., the agreement between values obtained at this laboratory and those of references 16 and 17), magnetic field strength, propellant mass flow rate and propellant type. Further, since different propellants have widely varying characteristic voltages (see, for example, figure 6), operation at a given current in two different propellants implies operation at different input power levels; therefore, electrode heat transfer is sensitive neither to mass flow rate nor to input power, and so it is insensitive, over the ranges plotted, to enthalpy.

    c.   The electrode heat transfer can be represented fairly well by a constant electrode voltage drop of approximately 26 volts.

    d.   On the basis of conclusions a through c, it would appear that convection is not a dominant process in transferring heat to the electrodes. Rather, some effect involving plasma sheaths and the electrode fall zones seems to be much more important.

With this understanding of the absolute magnitude of the electrode power losses in the X-2C MPD arcjet, the thermal efficiency data are readily

explained. Figure 12 shows, for hydrogen, thermal efficiency as a function of applied magnetic field strength. Mass flows of 0.02 and 0.05 gm/sec were used, with arc currents of 500, 600, 1,000, and 1,600 amperes. The solid symbols represent data obtained for the higher mass flow, and the dashed curves are drawn through these symbols. In general, based on figure 12, the thermal efficiency increases with current and magnetic field strength for the higher mass flow rate, and shows very little systematic variation with either current or magnetic field strength at the lower mass flow rate. In the range of parameters where the best propulsion performance has been obtained (high current, high magnetic field strength) the thermal efficiency varies between 65 and 75 percent. Referring to figure 4, it can be seen that the arc voltage shows only a slight dependence on current and on magnetic field strength at the 0.02 gm/sec mass flow rate, while it increases with magnetic field strength at the 0.05 gm/sec mass flow rate. Since the cooling power losses are essentially fixed by the arc current according to figure 7, the thermal efficiency is determined essentially by the arc voltage.

Figure 13 is drawn for ammonia and again plots thermal efficiency versus applied magnetic field strength for mass flow rates of 0.029 and 0.058 gm/sec and arc currents of 600, 1000, and 1400 amperes. There is some apparent tendency for the thermal efficiency to rise with current and magnetic field strength, and, at the higher currents, with mass flow rate. At the higher values of current and magnetic field strength, thermal efficiencies in the range 35 to 50 percent characterize the data.

Thus, the thermal efficiencies for ammonia are, under similar conditions, on the order of two-thirds of the thermal efficiencies in hydrogen. Referring again to figure 6, the same statement can be used to describe the operating voltage. The implications for overall propulsive efficiency are examined in a later section.

5. X-2C Thrust Characteristics

The variation of X-2C MPD arcjet thrust with current in the presence of a relatively small external magnetic field was investigated during the first quarter of this program, and was reported in detail in reference 4. Figure 14, taken from reference 4, shows the overall variation of thrust with current; also indicated in this figure is the behavior of T_{aero} with arc current. The difference between the total thrust and T_{aero} is assigned to the self-induced MPD thrust mechanisms of equations 2 through 5.

Figure 15 shows the variation of T_{Self}, defined as

$$T_{Self} = T_{Total} - T_{aero} \tag{10}$$

with current. Also shown on figure 15 are two theoretical predictions of T_{Self}, based upon two assumptions of the cathode current density distribution.
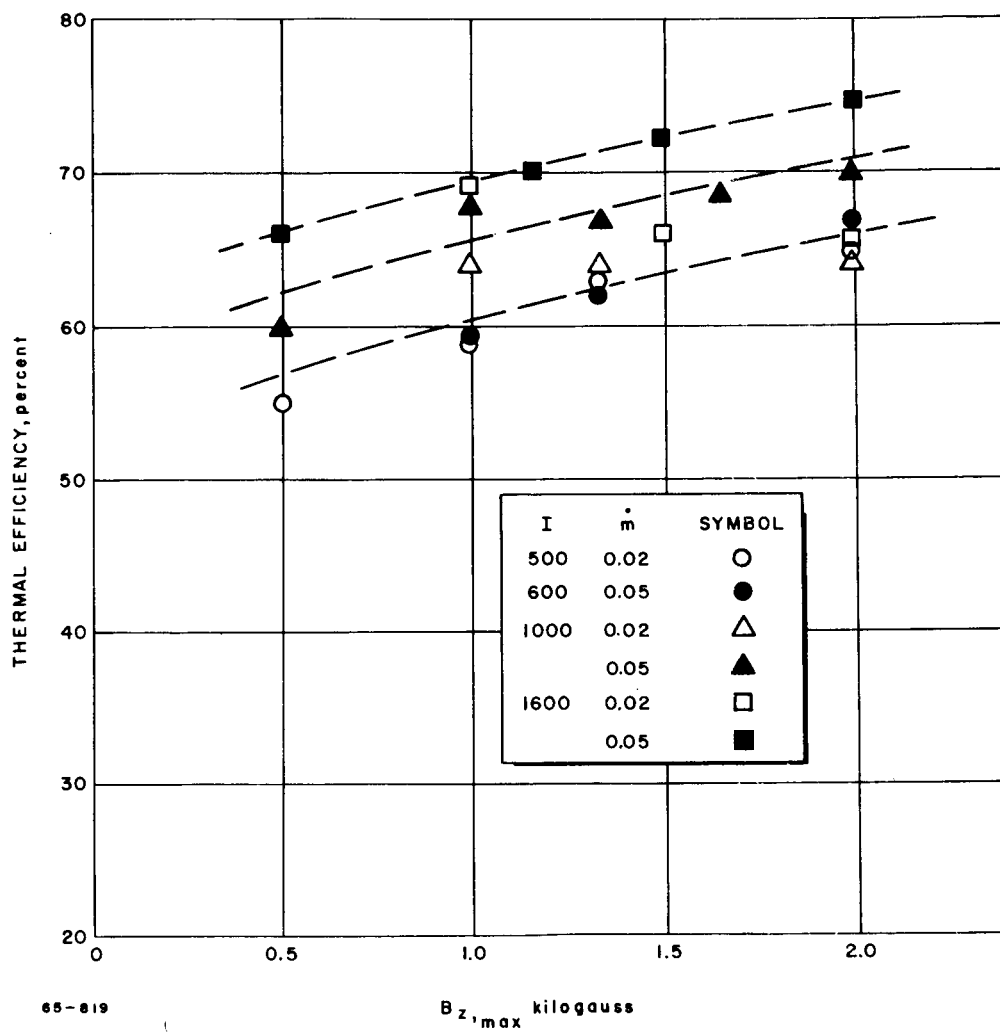
Figure 12 THERMAL EFFICIENCY VERSUS MAGNETIC FIELD STRENGTH (HYDROGEN)
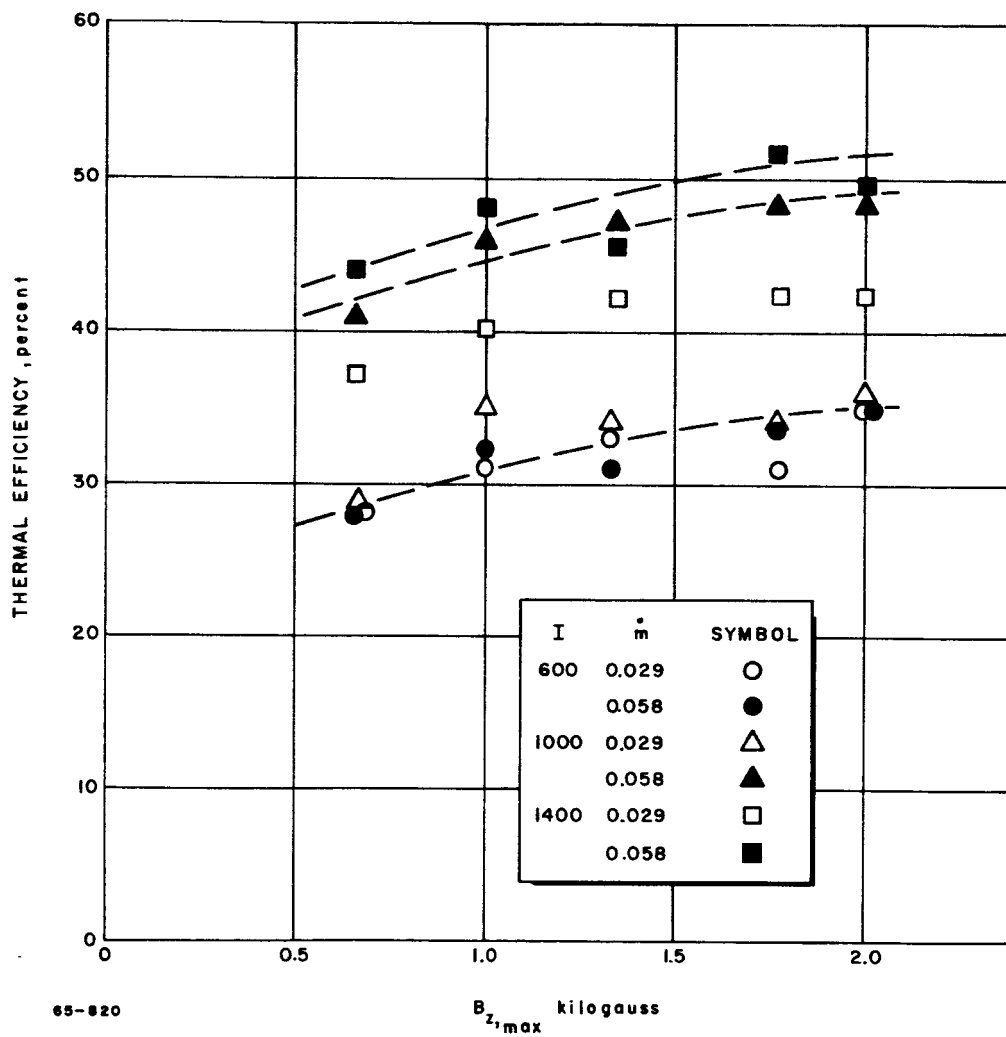
65-819

-24-

Figure 13 THERMAL EFFICIENCY VERSUS MAGNETIC FIELD STRENGTH (AMMONIA)

65-820
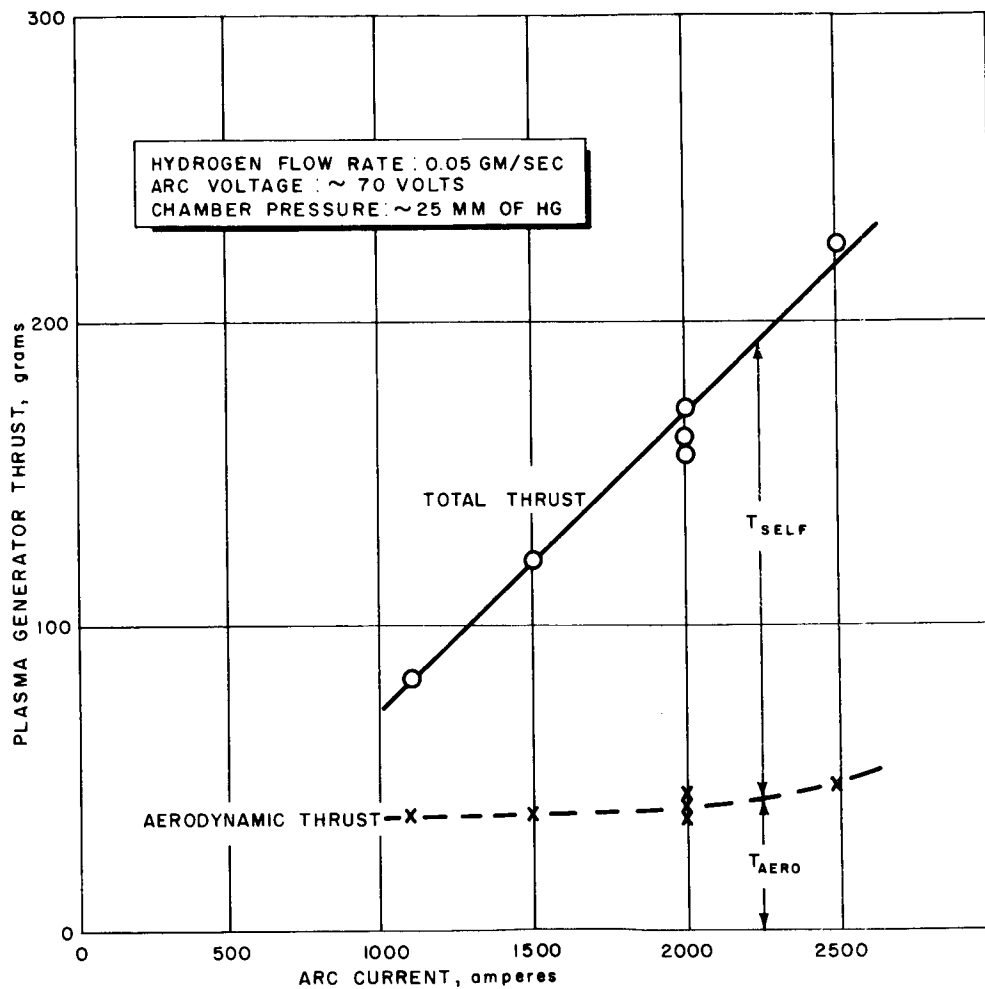
Figure 14   PLASMA GENERATOR THRUST VERSUS ARC CURRENT
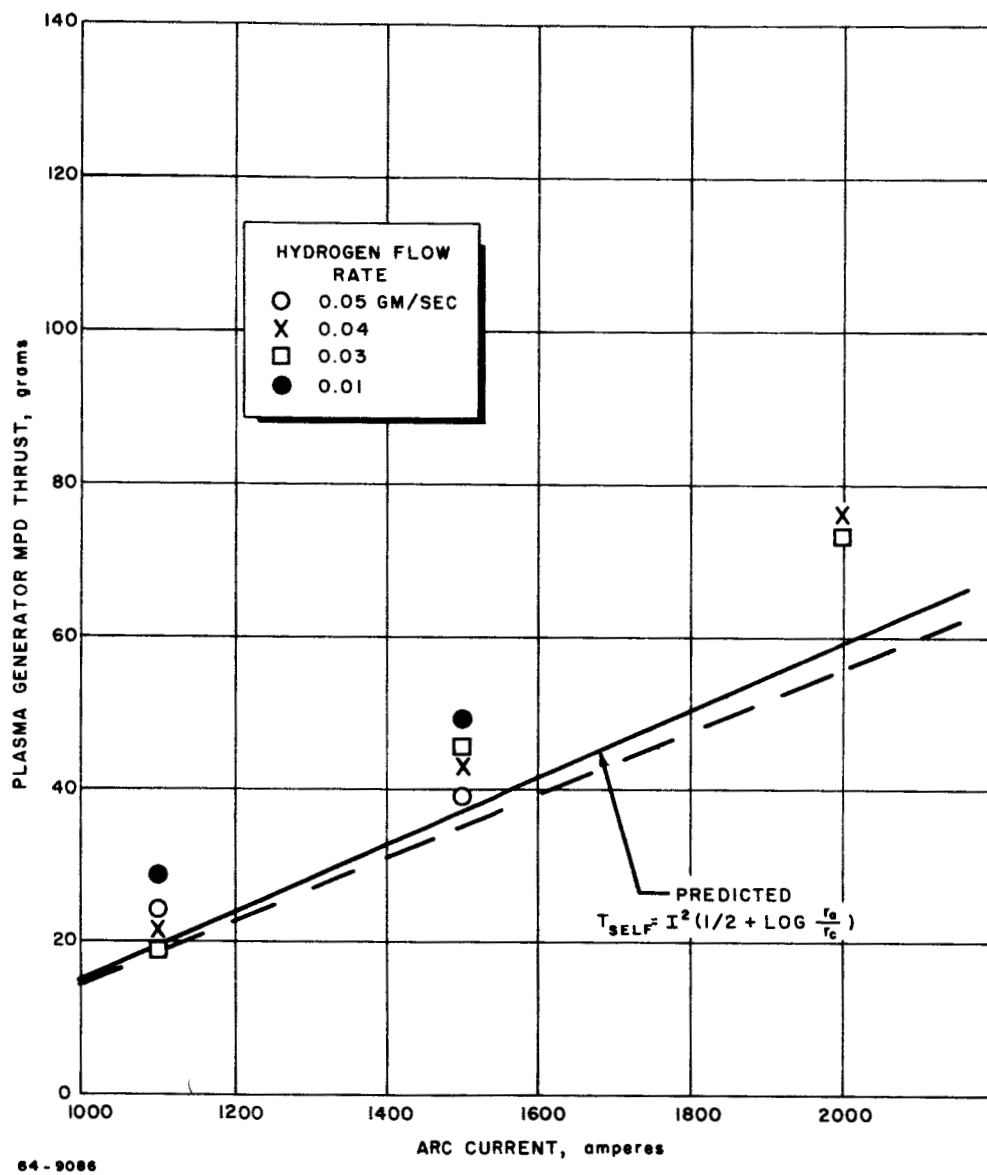
Figure 15 PLASMA GENERATOR SELF-THRUST VERSUS ARC CURRENT

64-9086

It can be seen from figure 15 that the theoretical predictions are in fairly good agreement with the measurements, but that they tend to be systematically low. It is now thought probable that the difference between the predictions and the measurements may be due to the Hall thrust mechanisms which were neglected in reference 4. Again it is pointed out that the self-induced MPD thrust comes from interactions between the applied current density and the self magnetic field, B_θ. When the applied magnetic fields B_r and B_z can produce circulating currents, j_θ, which are comparable in effect to the applied currents, then it is no longer even approximately correct to ignore the applied magnetic field.

Figure 16 is a plot of measured X-2C thrust as a function of arc current for a fixed strong field (the applied magnetic field is approximately 2,000 gauss, axial, maximum), and hydrogen mass flow rate (0.03 gm/sec). As the arc current is varied from 600 to 1600 amperes the thrust rises from 80 to 260 grams. Over this same current, range T_{aero} varies from 32 to 40 grams. If one uses equations 2, 3, and 4, for T_{Self} and the values reported in reference 4 for r_c, a curve to represent T_{Self} can be calculated and drawn. This is indicated in figure 16. However, the sum of T_{aero} and T_{Self} varies only between 40 and 95 grams over the current range 600 to 1,600 amperes, leaving the larger portion of the thrust unaccounted for. This excess of the thrust, the difference between the total measured thrust and the thrust which can be accounted for by the sum of T_{aero} and T_{Self}, is now assigned tentatively to Hall current acceleration.

It is not clear on a priori grounds what the dependence of Hall current thrust should be on an applied current and magnetic field, although it is anticipated that both parameters should be important in determining the magnitude of thrust. If the Hall current magnitude were proportional to $(\omega\tau)_e$ and hence to B, it would be expected that the thrust would vary roughly as I B^2; I and one power of B establish the Hall current magnitude, while another power of B is involved in determining the $\vec{j} \times \vec{B}$ force resulting. However, this assumes that the volume of interaction is independent of B (the thrust is a volume integral of $\vec{j} \times \vec{B}$) and this need not be so.

Hess[18] offers experimental evidence that in the range of currents, mass flow rates, and magnetic fields applicable to these experiments, the Hall current magnitude is relatively insensitive to B. If this were the case for the X-2C engine operation, the Hall thrust would become a linear function of I x B, assuming again that the volume over which the interaction takes place is not B-dependent.

In figure 17 the Hall thrust, defined as

$$T_{Hall} = T_{Total} - T_{aero} - T_{Self} \tag{11}$$

Figure 16 PLASMA GENERATOR THRUST VERSUS ARC CURRENT (HYDROGEN)
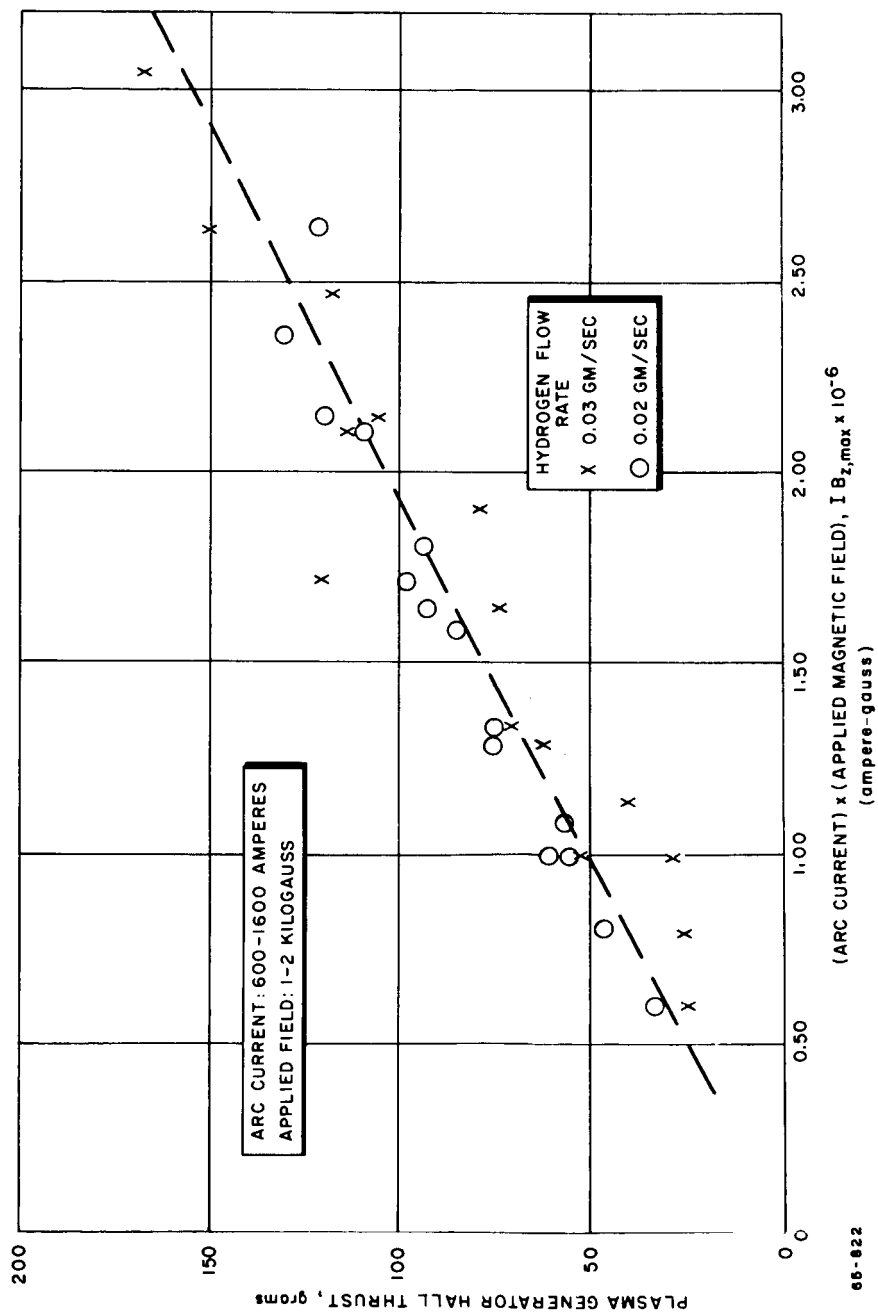
Figure 17 PLASMA GENERATOR HALL THRUST VERSUS PRODUCT OF ARC CURRENT AND MAGNETIC FIELD STRENGTH (HYDROGEN)

65-822

-30-

is plotted versus the product IB, where I is the total arc current and B is the axial field strength at the cathode tip. I varies from 600 to 1600 amperes and B from 1 to 2 kilogauss. Data for hydrogen mass flow rates of 0.02 and 0.03 gm/sec are included on the same figure. Although there is experimental scatter, the correlation is fairly good. T_{Hall} goes to zero for null values of the product IB and reaches approximately 160 grams at the peak IB value.

Figures 18 and 19 are drawn for X-2C operation with ammonia. In figure 18 overall thrust is plotted against arc current for applied magnetic field strength of approximately 2,000 gauss, axial, at the cathode tip. The ammonia mass flow rate is 0.029 gm/sec, and the arc current varies from 600 to 1,600 amperes. As in the case of figure 16 for the hydrogen data, the aerodynamic and self-MPD thrusts have been estimated and plotted on figure 18. The difference between the total measured thrust and that which can be accounted for by aerodynamic and self magnetic mechanisms alone is assigned, tentatively, to the Hall effect.

In figure 19 the Hall thrust deduced in this way, T_{Hall}, is plotted against the product of arc current and peak applied axial magnetic field strength. The correlation of T_{Hall} with IB is less satisfactory for ammonia (figure 19) than for hydrogen (figure 17). Perhaps more important, the magnitude of T_{Hall} is smaller in ammonia than in hydrogen at each value of IB; at the higher values of IB by a factor of 3 to 4. Hence, it appears that the applied magnetic field plays a smaller role in acceleration of ammonia than in acceleration of hydrogen. It has indeed already been noted that the arc voltage in ammonia is less sensitive to magnetic field than the arc voltage in hydrogen.

6. X-2C Efficiency

The overall propulsive efficiency is defined as the ratio of thrust power to input power:

$$\epsilon_o = \frac{4.8 \times 10^{-3} \ T^2}{\dot{m} \ P_{in}} = \frac{4.8 \times 10^{-3} \ T \ I_{sp}}{P_{in}} \tag{12}$$

where ϵ_o is the overall propulsive efficiency expressed in percent, T is the total thrust in grams, $\dot{m}$ the propellant mass flow rate in gm/sec, and I_{sp} the specific impulse in seconds. P_{in}, the input power, is taken as 10^{-3} I V, in kilowatts.

Figures 20 and 21 show, for hydrogen and for ammonia, the overall efficiency as a function of specific impulse.

Each figure includes data taken over a wide range of conditions; in figure 20, for hydrogen, the arc current varies approximately by a factor of 5 between 300 and 1,600 amperes, the applied magnetic field by a factor of
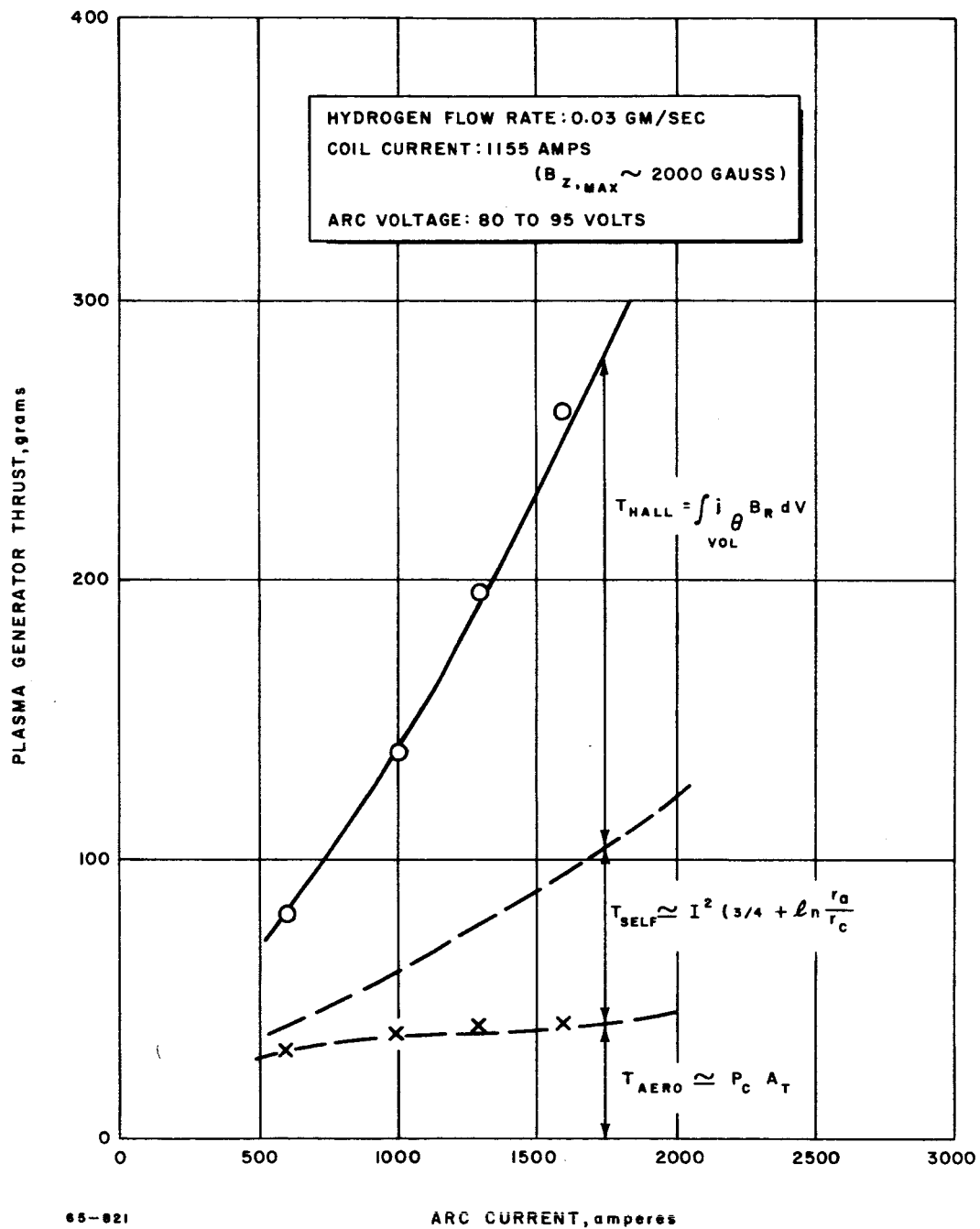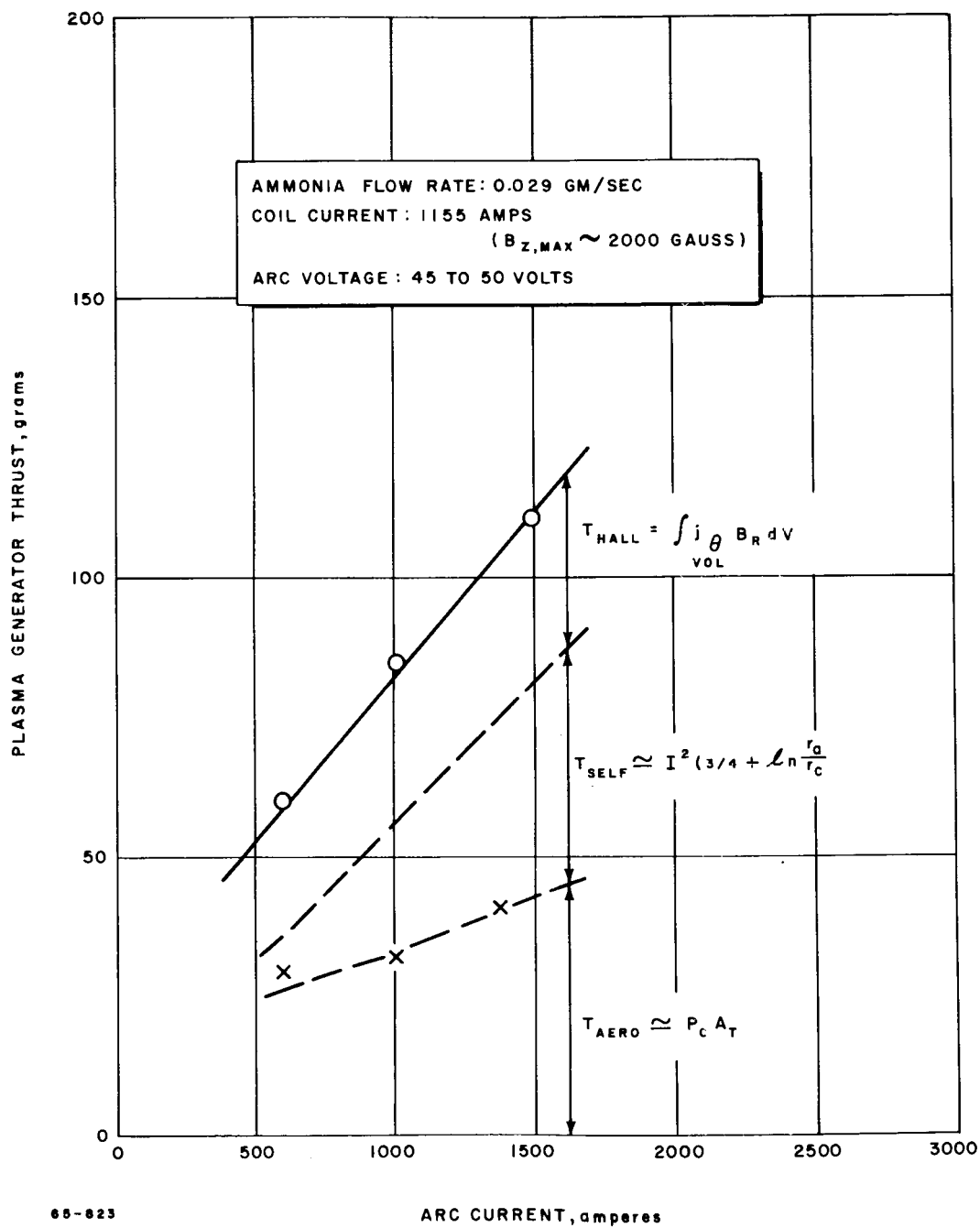
Figure 18 PLASMA GENERATOR THRUST VERSUS ARC CURRENT (AMMONIA)

65-823

- 32 -
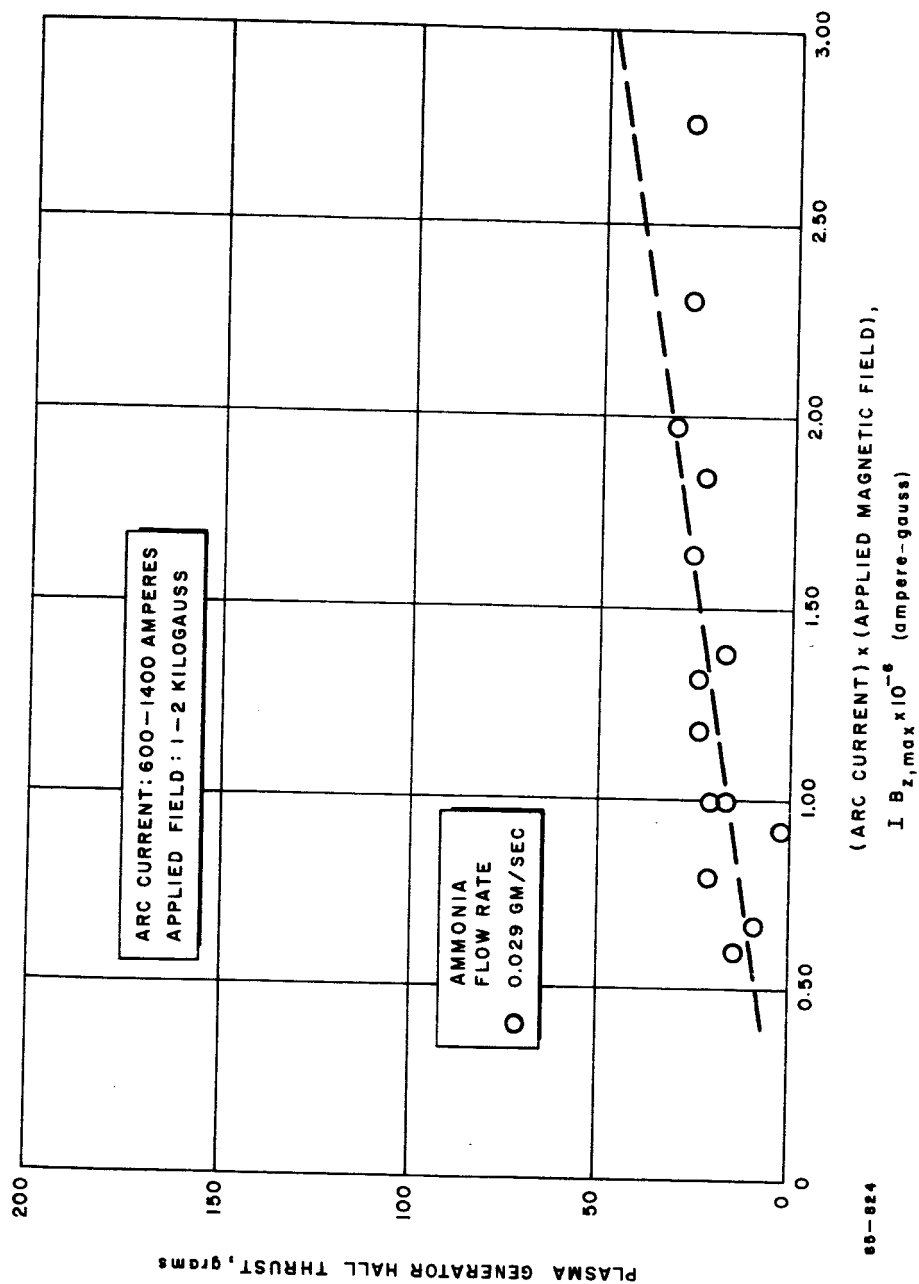
Figure 19 PLASMA GENERATOR HALL THRUST VERSUS PRODUCT OF ARC CURRENT AND MAGNETIC FIELD STRENGTH (AMMONIA)

85—824
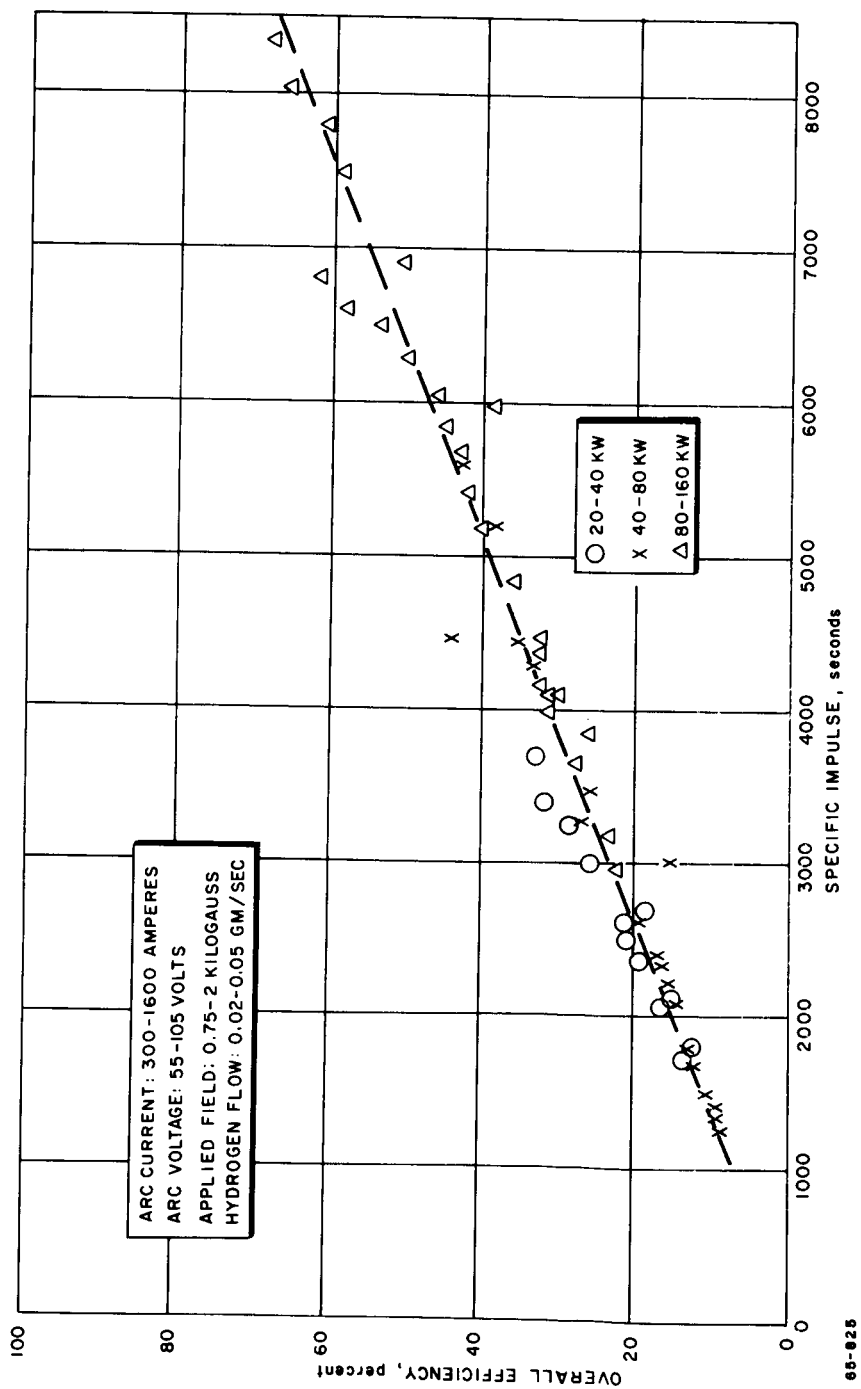
Figure 20 OVERALL EFFICIENCY VERSUS ARC ENGINE SPECIFIC IMPULSE (HYDROGEN)

ARC CURRENT: 300-1600 AMPERES
ARC VOLTAGE: 55-105 VOLTS
APPLIED FIELD: 0.75-2 KILOGAUSS
HYDROGEN FLOW: 0.02-0.05 GM/SEC

○ 20-40 KW
X 40-80 KW
△ 80-160 KW

SPECIFIC IMPULSE, seconds

OVERALL EFFICIENCY, percent

65-825

-34-
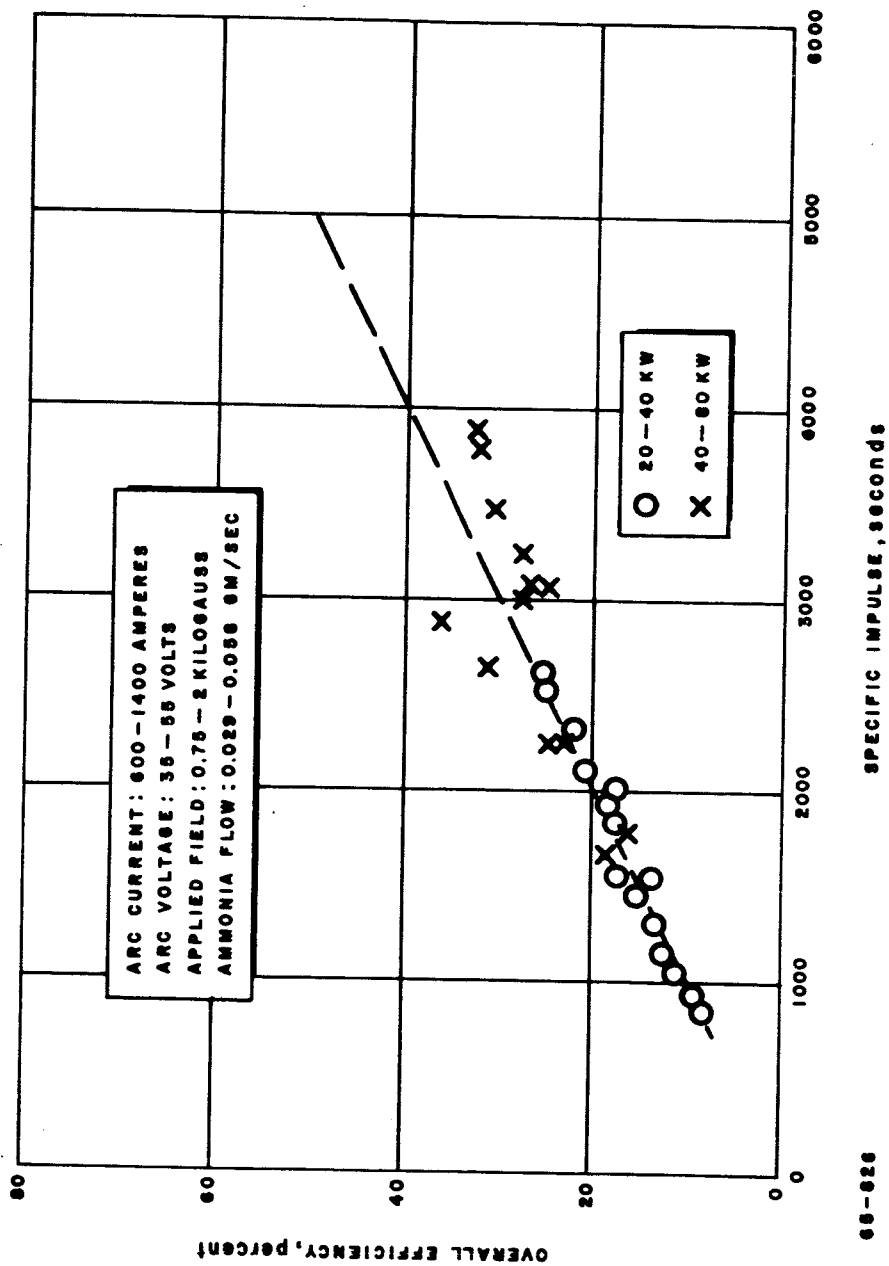
Figure 21 OVERALL EFFICIENCY VERSUS ARC ENGINE SPECIFIC IMPULSE (AMMONIA)

65-826

-35-

nearly 3 between 0.75 and 2 kilogauss, the propellant mass flow rate by a factor of 2.5 between 0.02 and 0.05 gm/sec, and the arc voltage by a factor of 2 between 55 and 105 volts. In figure 21, for ammonia, the variation is between 600 and 1,400 amperes in arc current, 0.75 and 2 kilogauss in applied magnetic field, 0.029 and 0.058 gm/sec in ammonia flow rate, and 35 and 55 volts in arc voltage.

Still, for each propellant, all the data on overall efficiency versus specific impulse fit very closely to a single curve. Within the range of parameters tested, the overall efficiency is then essentially a function only of I_{sp}, and not independently of field strength, power input, current, or propellant flow rate. To emphasize the independence of efficiency, at a given impulse, to input power level, the data of figures 20 and 21 have been coded so that different symbols apply to the different power ranges 20 to 40 kw, 40 to 80 kw, and 80 to 160 kw. Inspection of the figures indicates that the curves drawn to represent each power level are, within the experimental scatter, the same curves. It can be concluded, tentatively, that it should therefore be possible to achieve comparable efficiency-specific impulse curves at lower power levels than those which have been employed.

Figure 22 is drawn for comparison of hydrogen and ammonia in terms of overall propulsive efficiency. In each case the smooth curve is drawn to fit the data of figures 20 or 21, and the experimental scatter is indicated by the bars drawn on the ammonia curve. The indications of figure 22 are that the overall propulsive efficiency of the X-2C engine is somewhat higher in ammonia than in hydrogen by approximately 5 to 10 absolute points. That is, at a specific impulse of 4,000 seconds the efficiency with hydrogen is almost exactly 30 percent, while for ammonia the range 35 to 40 percent is indicated.

A partial explanation of this behavior can be sought by examining the overall efficiency in more detail. The overall efficiency can be written as a product of 3 subefficiencies; ϵ_{arc}, the heater efficiency; ϵ_f, the frozen flow efficiency; and ϵ_{exp}, the expansion efficiency:

$$\epsilon_{arc} = \frac{\text{Power to gas}}{\text{Power input}}$$

$$\epsilon_f = \frac{\text{Power available for thrust}}{\text{Power to gas}}$$

$$\epsilon_{exp} = \frac{\text{Thrust power}}{\text{Power available for thrust}}$$

$$\epsilon_o = \epsilon_{arc} \times \epsilon_f \times \epsilon_{exp}$$

Figure 22 OVERALL EFFICIENCY VERSUS ARC ENGINE SPECIFIC IMPULSE

65-827

-37-

ϵ_o and ϵ_{arc} are measured; ϵ_f and ϵ_{exp} must be estimated. Estimation of the frozen flow efficiency is difficult, since the enthalpy level at which freezing occurs is unknown. A considerable portion of the input energy is inserted directly in the kinetic form, so that the static enthalpy need not be excessively high. Estimation of the expansion efficiency is equally difficult, since the factors which contribute to this efficiency (velocity profile loss, angular spread, failure to convert random to directed motion, etc.) are closely tied to the acceleration mechanisms, which are themselves not understood in detail. However, two simplifying assumptions may be made which permit comparison of the hydrogen and ammonia efficiency data. These assumptions are crude, but satisfactory for the present stage of understanding of MPD arcjet behavior. The first assumption is

$$\epsilon_{exp, H_2} \approx \epsilon_{exp, NH_3} \qquad \text{for} \quad 1000 \text{ sec} < I_{sp} < 5000 \text{ sec}$$

That is, the fraction of input power which is lost in velocity profiles, etc., is the same for hydrogen and ammonia at any given specific impulse in the range 1,000 to 5,000 seconds. This range of specific impulse is the range where overlapping data in hydrogen and ammonia are available.

The second assumption involves the frozen flow efficiency. Here it is assumed that the percentage of dissociation and ionization for hydrogen and ammonia are the same at a given specific impulse; e.g., if hydrogen is 10 percent ionized at 2,000 seconds, then ammonia is also 10 percent ionized at this specific impulse. Then, approximately, the ratio $\epsilon_{f, H_2}/\epsilon_{f, NH_3}$ at a given I_{sp} is the same as the ratio which would hold for full ionization even though it is not at all necessary that ϵ_{f, H_2} or ϵ_{f, NH_3} represent full ionization.

With these assumptions, the overall efficiency ratio for ammonia and hydrogen can be written

$$\frac{\epsilon_{o, NH_3}}{\epsilon_{o, H_2}} = \frac{\epsilon_{arc, NH_3}}{\epsilon_{arc, H_2}} \times \frac{\epsilon_{f, NH_3}}{\epsilon_{f, H_2}}$$

Table I evaluates this ratio and compares it with that experimentally obtained. Data on ϵ_f are taken from figure 23, which assumes full dissociation and 1st ionization of all atoms.

Agreement between the overall efficiency ratios calculated in this fashion and those measured is fairly good, except at the lowest specific impulse value, 2,000 seconds. At the lower values of I_{sp} the calculation of ϵ_f is expected to be particularly crude, so that this result is not surprising.

Figure 22 OVERALL EFFICIENCY VERSUS ARC ENGINE SPECIFIC IMPULSE

65-827

-37-

ϵ_o and ϵ_{arc} are measured; ϵ_f and ϵ_{exp} must be estimated. Estimation of the frozen flow efficiency is difficult, since the enthalpy level at which freezing occurs is unknown. A considerable portion of the input energy is inserted directly in the kinetic form, so that the static enthalpy need not be excessively high. Estimation of the expansion efficiency is equally difficult, since the factors which contribute to this efficiency (velocity profile loss, angular spread, failure to convert random to directed motion, etc.) are closely tied to the acceleration mechanisms, which are themselves not understood in detail. However, two simplifying assumptions may be made which permit comparison of the hydrogen and ammonia efficiency data. These assumptions are crude, but satisfactory for the present stage of understanding of MPD arcjet behavior. The first assumption is

$$\epsilon_{exp, H_2} \approx \epsilon_{exp, NH_3} \qquad \text{for} \quad 1000 \text{ sec} < I_{sp} < 5000 \text{ sec}$$

That is, the fraction of input power which is lost in velocity profiles, etc., is the same for hydrogen and ammonia at any given specific impulse in the range 1,000 to 5,000 seconds. This range of specific impulse is the range where overlapping data in hydrogen and ammonia are available.

The second assumption involves the frozen flow efficiency. Here it is assumed that the percentage of dissociation and ionization for hydrogen and ammonia are the same at a given specific impulse; e.g., if hydrogen is 10 percent ionized at 2,000 seconds, then ammonia is also 10 percent ionized at this specific impulse. Then, approximately, the ratio $\epsilon_{f, H_2}/\epsilon_{f, NH_3}$ at a given I_{sp} is the same as the ratio which would hold for full ionization even though it is not at all necessary that ϵ_{f, H_2} or ϵ_{f, NH_3} represent full ionization.

With these assumptions, the overall efficiency ratio for ammonia and hydrogen can be written

$$\frac{\epsilon_{o, NH_3}}{\epsilon_{o, H_2}} = \frac{\epsilon_{arc, NH_3}}{\epsilon_{arc, H_2}} \times \frac{\epsilon_{f, NH_3}}{\epsilon_{f, H_2}}$$

Table I evaluates this ratio and compares it with that experimentally obtained. Data on ϵ_f are taken from figure 23, which assumes full dissociation and 1st ionization of all atoms.

Agreement between the overall efficiency ratios calculated in this fashion and those measured is fairly good, except at the lowest specific impulse value, 2,000 seconds. At the lower values of I_{sp} the calculation of ϵ_f is expected to be particularly crude, so that this result is not surprising.
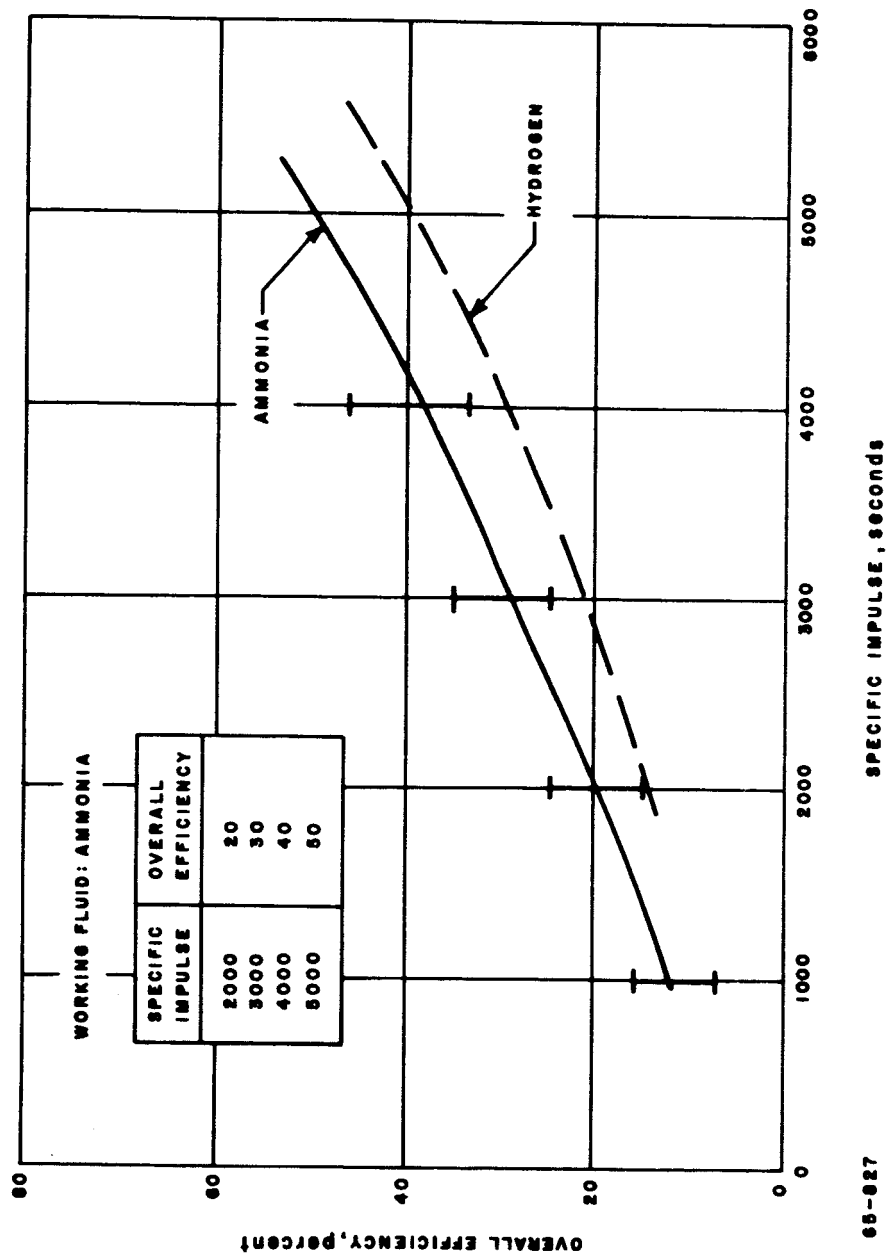
Figure 23   FROZEN FLOW EFFICIENCY VERSUS ARC ENGINE SPECIFIC IMPULSE

64-10348

TABLE I

OVERALL EFFICIENCY RATIO FOR AMMONIA AND HYDROGEN

I_{sp} (seconds)	$\epsilon_{arc,\,NH_3}$ (percent)	$\epsilon_{arc,\,H_2}$ (percent)	$\dfrac{\epsilon_{f,\,NH_3}}{\epsilon_{f,\,H_2}}$	$\dfrac{\epsilon_{o,\,NH_3}}{\epsilon_{o,\,H_2}}$ (calculated)	$\dfrac{\epsilon_{o,\,NH_3}}{\epsilon_{o,\,H_2}}$ (measured)
2000	42	65	3.04	1.9	1.4
3000	42	65	2.42	1.5	1.4
4000	42	65	1.97	1.3	1.3
5000	42	65	1.72	1.1	1.2

The results of table I indicate that, at least to first order, the overall efficiency data for hydrogen and ammonia can be compared on the basis that the expansion efficiency is essentially the same for the two propellants, and that the differences in overall efficiency can be attributed to the arc and frozen flow efficiencies.

C. CONCLUSIONS AND FUTURE EFFORT

1. Conclusions

a. The X-2C MPD arcjet engine has been operated over a broad range of arc current, applied magnetic field strength, and propellant mass flow rate, in hydrogen and in ammonia.

b. For each propellant the overall efficiency appears to be a nearly unique function of specific impulse level. For ammonia, the overall efficiency is approximately 20 percent at 2000 seconds, 30 percent at 3000 seconds, and 35 percent at 3500 seconds. For hydrogen, the overall efficiency is approximately 15 percent at 2000 seconds, 20 percent at 3000 seconds, 30 percent at 4000 seconds, and 40 percent at 5000 seconds.

c. The efficiencies appear to be independent of input power level in the range explored. (20 to 160 kw)

d. X-2C performance has been accounted for in terms of thrust mechanisms; aerodynamic, self-magnetic, and Hall current acceleration. The Hall current thrust appears to be proportional to the product IB of the arc current and applied magnetic field strength, while the self-magnetic thrust is proportional to I^2.

e. The power lost to the electrodes appears to be primarily a function of arc current, and is consistent with an electrode fall voltage (for heating)

of about 25 volts in hydrogen, ammonia, nitrogen, helium, and argon. This is not characteristic of convective heating. The possibility thus arises that the propellant is in some degree magnetically contained, and that operation in a hard vacuum may not be appreciably different than in the laboratory.

f.   The thermal or arc efficiency is typically about 40 percent for ammonia and 65 percent for hydrogen. The thermal efficiency tends to increase with current and magnetic field strength, but large variations have not been observed over the currents and magnetic field strengths employed.

g.   The arc voltage tends to increase with applied magnetic field strength, approximately in the way predicted by Patrick and Schneidermann.[15]

h.   The relative overall efficiencies in hydrogen and ammonia can be accounted for on the basis that the expansion efficiencies for the two propellants are equal, and that the degree of ionization is also approximately the same. The energy balance indicates that the ionization is significantly less than complete; indeed, a degree of ionization in the range 2 to 20 percent seems to account best for the data.

2.   Future Effort

The conclusions which have been reached as a result of the work so far performed under this program, as well as the interchange of information at the MPD Arcjet Thrustor Conference,* indicate a number of paths of future research to develop the MPD arc into a practical propulsion device compatible with solar cell power supplies. In order that the thrustor be compatible with solar cell power supplies, it appears essential that effort be concentrated at power levels below 50 kw. The indications of the work reported here are that this should not greatly affect the efficiency- I_{sp} curve, at least at power levels down to 10 kw. The ammonia efficiency is greater at each I_{sp} than the hydrogen efficiency; emphasis on further development work with storable ammonia is called for. In addition, exploration of MPD arcjet thrustor performance with one of the alkali metals may yield efficiency increases owing to frozen flow considerations. Along this line, potassium seems worthy of consideration since it combines high frozen flow efficiency in the interesting I_{sp} range (over 90 percent at $I_{sp} > 1500$ seconds, even for full first ionization) with ease of handling compared to other alkali metals (e.g., lithium).

---

* Held at NASA LeRC, 17 December 1964.

The use of a heavy propellant such as ammonia or potassium at low power levels may cause a problem which has not been experienced so far in hydrogen or at higher powers. That is, the acceleration of the bulk of the propellant appears to be through collisions and is therefore dependent to some degree on particle number density. As the propellant molecular weight is raised (to enhance frozen flow efficiency) and the propellant mass flow rate is decreased (to allow low power operation), this number density decreases unless the device scale is reduced. The question then arises as to whether a device can be built on a sufficiently small scale to keep the particle number density high, while handling input power levels on the order of a few to a few tens of kilowatts. This question can best be answered in the laboratory.

Two other aspects of research appear necessary for practical realization of the MPD arcjet thrustor. These are 1) operation with radiation cooling and 2) study of the state of the art in magnet construction. It appears that the self-magnetic thrust mechanisms are not readily adapted to low-power thrustor operation (high currents are required, and even the electrode fall voltages themselves multiplied by these currents give appreciable power levels; this restriction at low power has also been pointed out by Stratton[*] and by Ashly and Gooding[*]), so that a low-power MPD arc will require a substantial external magnetic field. While in principle a permanent magnet may be used, it is not clear in practice what weight penalties are associated with permanent magnets and electromagnets.

The use of radiation cooling would of course be a great simplification over liquid cooling. It will be possible to make use of technology developed under previous 30-kw radiation cooling programs.

Finally, while a considerable amount of testing has been completed here by varying the magnetic field strength, there has been no attempt to change the ratio B_z to B_r. Patrick[*] indicates that this ratio is critical, and reports promising propulsion data obtained with a particular field configuration. On the other hand, the similarity between the data obtained here and those of Cann and of Hess tend to deemphasize the importance of field shape. Some experimentation with variation of the field configuration should clarify this point.

---

[*]Held at NASA LeRC, 17 December 1964.

III. 30-KW ARCJET LIFETESTS AND PULSED PERFORMANCE

The 30-kw thermal arcjet engine anode consists of a tungsten alloy nozzle section joined to a molybdenum plenum section. Best results in joining these two sections have been achieved with diffusion bonding and brazing.

For a lifetest of the 30-kw engine, a nozzle section has been fabricated of 75 percent tungsten and 25 percent rhenium. This material proved to have useful high temperature properties on an earlier 3-kw Resistojet program.

After a preliminary bonding investigation utilizing small samples of the 75 percent W - 25 percent Re, and molybdenum, it was decided to use a basic diffusion bond along with an exterior chrome-vanadium braze.

The first attempt to bond a full scale nozzle-plenum structure failed when bonding material plugged several of the propellant inlet orifices. The molybdenum plenum was then machined away from the nozzle, a new plenum section was fabricated, and a successful bond has been obtained.

The engine is now nearly ready for the lifetest, which has been scheduled for the next quarter.

IV. PROGRAM DIRECTION

1. The 30-kw radiation cooled thermal arcjet engine has been rebrazed. The lifetest is rescheduled for the third quarter.

2. Experimental attention in the MPD area will be directed toward operation of a low-power ($<$50-kw) radiation cooled design with particular emphasis on operation with ammonia.

3. Fabrication of an alkali metal feed system will be continued, with provision for handling alkali metal vapors in the test tank.

4. Studies will be made of the magnet state of the art, with particular emphasis on weight penalties attaching to permanent and electromagnets.

5. Some variation of the B_z/B_r ratio will be attempted, and effects on propulsion performance investigated.

6. With the currently available improved vacuum facility, many of the data points obtained with 100-micron blankoff pressure will be rerun, and the effect of blankoff pressure checked.

V. REFERENCES

1. Ducati, A. C., G. M. Gianni, and E. Muehlberger, Experimental Results in High-Specific-Impulse Thermo-Ionic Acceleration, AIAA J. 2, 1452 (1964).

2. Schoeck, P. A., The Magnetohydrodynamic Arc Thrustor, ARO Internal Report (August 1964).

3. Cann, G. L., Annular Magnetic Hall Current Accelerator, AIAA Paper 64-670 (1964).

4. Avco RAD, Arcjet Technology Research and Development, First Quarterly Progress Report RAD-SR-64-239, on Contract No. NAS 3-5900 (October 1964).

5. Maecker, H., Plasmaströmungen in Lichtobögen infolge ergen magnetischer Kompression, Z. Phys., 141, 198 (1955).

6. Hess, R. V., Experiments and Theory for Continuous Steady Acceleration of Low Density Plasmas, Proceedings of the XI International Astronautical Congress, Stockholm, Volume I, pp. 404-411 (1960).

7. Hess, R. V., Fundamentals of Plasma Interaction with Electric and Magnetic Fields, Proceedings of the NASA - University Conference on the Science and Technology of Space Exploration, Paper No. 59, Volume 2 (November 1963).

8. Ellis, M. C., Jr., Survey of Plasma Accelerator Research, Proc. NASA - University Conference, Paper No. 62 (November 1963).

9. Powers, W. E. and R. M. Patrick, A Magnetic Annular Arc, Avco Everett Research Laboratory Report RR-129 (May 1962).

10. Seikel, G. R. and E. Reshotoko, Hall Current Ion Accelerator, Bul. Am. Phys. Soc., 7, No. 6 (1962).

11. Cann, G. L., J. M. Teem, R. D. Buhler, and C. K. Branson, Magneto-gasdynamic Accelerator Techniques, AEDC-TDR-62-145 (July 1963).

12. Cann, G. L. and G. L. Marlotte, Hall Current Plasma Accelerator, AIAA J., 2, 1234 (1964).

13. Patrick, R. M. and W. E. Powers, Plasma Flow in a Magnetic Arc Nozzle, Third Symposium on Advanced Propulsion Concepts, Cincinnati, Ohio (October 1964).

14. Brandmaier, A. E., J. L. Durand, M. C. Gourdine, and A. Rubel, An Investigation of Hall Propulsor Characteristics, AIAA J., 2, 674 (1964).

15. Patrick, R. M., Study of Magnetic Annular Plasma Accelerator, Second Quarterly Progress Report on Contract No. NAS 3-5748 (September 1964).

16. Cann, G. L., P. D. Lenn and R. L. Harder, Hall Current Accelerator, EOS Report 5470-QL-1, First Quarterly Progress Report on Contract No. NAS 3-5909 (October 1964).

17. Ducati, A. C., E. Muelberger, and J. P. Todd, Design and Development of a Thermo-Ionic Electric Thrustor, Giannini Scientific Corp. Interim Report on Contract No. NAS w-968 (September 1964).

18. Grossman, W., R. V. Hess and H. A. Hassan, Experiments with a Coaxial Hall Current Plasma Accelerator, AIAA Paper No. 64-700 (1964).

APPENDIX

MPD ARCJET ENGINE PERFORMANCE DATA

MPD ARCJET ENGINE PERFORMANCE DATA

Tables II, III, and IV list performance values which have been obtained with the X-2C MPD engine in hydrogen at mass flows of 0.05, 0.03, and 0.02 gm/sec, respectively. Tables V and VI list the performance values obtained in ammonia at mass flows of 0.058 and 0.029 gm/sec, respectively.

TABLE II

PERFORMANCE OF THE MPD ARC X-2C WITH HYDROGEN MASS FLOW OF 0.05 GM/SEC

Arc Current (amperes)	Field Coil Current (amperes)	Arc Voltage (volts)	Thrust (grams)	Specific Impulse (seconds)	Input Power (kw)	Thrust Efficiency (percent)	Power to Anode and Cathode (kw)	Thermal Efficiency (percent)
600	700	72	62	1240	43.3	8.5	18.7	57
1000		70.5	104	2080	70.5	14.8	26.8	62
1300		70.5	146	2920	91.7	22.3	32.0	65
1600		81	204	4080	129.5	30.9	38.3	70
600	800	76	66	1320	45.6	9.2	20.3	55
1000		76	116	2320	76.0	17.0	28.2	63
1300		80	158	3160	104.0	23.1	33.8	68
1600		86	216	4320	137.5	32.6	39.3	71
600	900	80	70	1400	48.0	9.8	20.7	57
1000		80.5	120	2400	80.5	17.1	29.1	64
1300		85	174	3840	110.5	26.3	34.7	69
1600		90	222	4440	144.0	32.8	40.2	72
600	1000	85	74	1480	51.0	10.3	21.7	57
1000		85	129	2580	85.0	17.8	30.0	65
1300		90	183	3660	117.0	27.5	36.5	69
1600		95	241	4820	152.0	36.7	41.2	73
600	1100	88.5	83	1660	53.1	12.5	22.6	57
1000		90	145	2900	90.0	22.4	31.0	66
1300		95	200	4000	123.5	31.1	37.4	70
1600		100	258	5160	160.0	40.0	41.6	74
600	1200	92	87	1740	55.2	13.2	22.6	59
1000		94	149	2980	94.0	22.6	31.9	66
1300		99	208	4160	129.0	32.2	37.9	71
1600		103.5	270	5400	166.0	42.2	42.6	74

TABLE III

PERFORMANCE OF THE MPD ARC X-2C WITH HYDROGEN MASS FLOW OF 0.03 GM/SEC

Arc Current (amperes)	Field Coil Current (amperes)	Arc Voltage (volts)	Thrust (grams)	Specific Impulse (seconds)	Input Power (kw)	Thrust Efficiency (percent)	Power to Anode and Cathode (kw)	Thermal Efficiency (percent)
600	600	65.5	58	1930	39.3	13.7	17.2	56
1000		67	104	3460	67.0	25.8	25	63
1300		65.5	129	4300	85.0	31.3	29.7	65
1600		89	234	7810	143	61.2	36.7	74
600	700	70	62	2070	42.0	14.7	16.4	61
1000		75	121	4030	75.0	31.2	25.4	66
1300		83	175	5830	107.7	45.5	31.5	71
1600		91	250	8320	146	68.5	37.1	75
600	800	75	66	2200	45.0	15.5	18.5	59
1000		80	129	4300	80	33.3	26.9	66
1300		85.5	188	6260	111	51.0	33.0	70
1600		70	195	6500	112	54.4	37.0	67
600	900	79	70	2330	47.4	16.5	18.9	60
1000		80	133	4420	80	35.4	28.8	64
1300		83.5	179	5960	108.5	39.4	34.6	68
1600		87.5	241	8020	140	66.5	39.3	72
600	1000	82.5	74	2460	49.5	17.7	19.8	60
1000		82.5	133	4430	82.5	34.2	29.9	64
1300		86.5	181	6030	112	46.8	36.0	68
1600		90.0	245	8160	144	66.6	40.4	72
600	1100	85	78	2600	51	19.1	20.4	60
1000		85.5	141	4700	85.5	37.2	31.3	63
1300		87.5	197	6560	104	59.7	35.6	66
1000	1200	83	139	4620	83	37.2	30.0	64
600		87.5	80	2660	52.5	19.5	20.4	61

TABLE IV

Arc Current (amperes)	Field Coil Current (amperes)	Arc Voltage (volts)	Thrust (grams)	Specific Impulse (seconds)	Input Power (kw)	Thrust Efficiency (percent)	Power to Anode and Cathode (kw)	Thermal Efficiency (percent)
300	400	59	26	1300	17.7	9.0	7.9	55
400		56	34	1700	22.4	12.5	10.4	54
500		56	42	2100	28.0	15.0	11.8	58
300	600	62.5	28	1400	18.8	10.1	7.9	58
400		62	36	1800	24.8	12.5	13.0	48
500		61.5	52	2600	30.8	21.1	12.3	60
600		62.5	54	2700	37.5	18.7	16.2	57
1000		67	104	5200	67.0	38.7	24.2	64
1300		70	138	6900	91.0	50.2	29.5	68
1600		65	159	7950	104	58.3	35.6	66
600	700	68	65	3250	40.8	27.2	17.1	58
1000		70	112	5600	70.0	43.0	25.0	64
1300		70	150	7500	91.0	59.3	30.7	66
300	800	70	34	1700	21.0	13.3	8.8	58
400		71.5	50	2500	28.6	21.0	11.5	60
500		71	65	3250	35.5	28.3	13.6	62
300	1000	80	41	2050	24.0	16.7	9.2	62
400		80	60	3000	32.0	26.9	12.0	63
500		79.5	74	3700	39.8	33.0	14.6	63
300	1200	86	47	2350	25.8	19.8	9.7	62
400		86	68	3400	34.4	32.0	12.5	64
500		85	89	4450	42.5	44.5	15.1	66

TABLE V

PERFORMANCE OF THE MPD ARC X-2C WITH AMMONIA MASS FLOW OF 0.058 GM/SEC

Arc Current (amperes)	Field Coil Current (amperes)	Arc Voltage (volts)	Thrust (grams)	Specific Impulse (seconds)	Input Power (kw)	Thrust Efficiency (percent)	Power to Anode and Cathode (kw)	Thermal Efficiency (percent)
600	350	38	48	830	22.8	8.3	15.1	34
	400	40.5	51	880	24.3	9.1	15.1	38
	600	44.5	61	1050	26.7	11.6	15.6	42
	800	47	66	1140	28.2	12.8	16.5	41
	1000	50	65	1120	30.0	11.7	17	43
	1200	54	74	1275	32.4	13.9	17.9	45
800	340	38	57	980	30.4	8.9	20	34
	400	40	64	1100	32	10.6	20	37
	600	43	74	1275	34.4	13.1	20	42
	800	45	83	1430	36.0	15.8	20.9	42
	1000	47	89	1535	37.6	17.3	21.9	42
	1200	51	95	1640	40.8	18.1	22.8	44
1000	300	39	52	895	39	5.6	23.8	39
	400	40.5	59	1020	40.5	7.2	23.8	41
	600	44	74	1275	44	10.2	23.8	46
	800	46	84	1450	46	12.6	24.2	47
	1000	48.5	90	1550	48.5	13.8	25.2	48
	1200	50	100	1725	50	16.6	26.1	48
1200	300	39	74	1280	46.8	9.6	27.1	42
	400	40	85	1465	48	12.5	27.1	44
	600	43	100	1725	51.7	16.0	27.6	47
	800	45	110	1900	54	17.0	28.1	48
	1000	49	120	2070	59	20.4	29	51
	1200	50	130	2240	60	23.4	30.4	49
1400	300	39	124	2140	54.6	23.2	31.5	42
	400	40	129	2220	56	24.4	31.1	44
	600	43	152	2620	60.2	31.8	31.3	48
	800	45	166	2860	63	36.2	34.3	46
	1000	48	176	3030	67.2	38.0	32.7	51
	1200	50	186	3200	70	41.0	35.6	49

TABLE VI

PERFORMANCE OF THE MPD ARC X-2C WITH AMMONIA MASS FLOW OF 0.029 GM/SEC

Arc Current (amperes)	Field Coil Current (amperes)	Arc Voltage (volts)	Thrust (grams)	Specific Impulse (seconds)	Input Power (kw)	Thrust Efficiency (percent)	Power to Anode and Cathode (kw)	Thermal Efficiency (percent)
600	400	37.5	38	1310	22.5	10.7	16.2	28
	600	40.5	44	1520	24.3	13.1	16.7	31
	800	43	53	1830	25.8	17.8	17.2	33
	1000	45	56	1930	27.0	19.3	18.6	31
	1200	49	61	2100	29.4	20.8	19.1	35
800	400	35	52	1790	28	16.1	19.1	32
	600	40	58	2000	32	17.5	21	34
	800	42	67	2310	33.6	22	21.5	36
	1000	44	73	2520	34.2	25	22.9	35
	1200	46	75	2590	36.8	25.3	23.9	35
1000	400	35	55	1900	35	14.3	25	29
	600	39	66	2280	39	18.5	25.5	35
	800	41	75	2580	41	22.6	26.9	34
	1000	43	81	2790	43	25.2	27.8	35
	1200	45	87	3000	45	27.8	28.7	36
1200	400	35	59	2040	42	13.8	28.7	32
	600	38.5	74	2550	46.2	19.7	28.7	38
	800	41.5	88	3040	49.8	25.7	29.8	40
	1000	44	94	3240	52.9	27.7	31.6	40
	1200	45	100	3450	54.0	30.6	32.6	40
1400	400	35	68	2345	49	15.6	30.7	37
	600	37.5	89	3070	52.5	24.9	31.6	40
	800	40	100	3450	56	29.4	32.6	42
	1000	43.5	111	3830	60.9	33.6	35.4	42
	1200	45	112	3860	63	32.8	36.4	42

DISTRIBUTION

Addressee	No. of Copies
NASA Lewis Research Center Mail Stop 21-5 2100 Brookpark Road Cleveland, Ohio 44135 Attn: H. Hunczak	5
NASA-Langley Research Center Library Hampton, Virginia 23365	1
NASA Lewis Research Center Spacecraft Tech. Procurement Sec. 2100 Brookpark Road Cleveland, Ohio 44135	1
NASA Lewis Research Center Library 21000 Brookpark Road Cleveland, Ohio 44135	1
NASA Lewis Research Center 21000 Brookpark Road Cleveland, Ohio 44135 Attn: J. Jack	1
NASA Ames Research Center Library Moffett Field, California 94035 Attn: Dr. G. Goodwin	1
NASA Ames Research Center Library Moffett Field, California 94035	1

Addressee	No. of Copies

NASA
Goddard Space Flight Center
Greenbelt, Maryland 20771
Attn: W. Isley, Code 623,
Bldg. 6   1

NASA
Marshall Space Flight
R-Rp-DIR
Bldg. 4481
Huntsville, Alabama, 35812   1

NASA
Marshall Space Flight Center
R-RP-T
Bldg. 4488
Huntsville, Alabama, 35812
Attn: W. Jones   1

NASA
Marshall Space Flight Center
R-RP-DIR
Huntsville, Alabama 35812
Attn: Dr. E. Stuhlinger   1

NASA Headquarters
FOB-10B
600 Independence Ave. N.W.,
Washington, D.C.
Attn: RNT/J. Lazar   2

Commander
Aeronautical System Division
Wright-Patterson AFB, Ohio
45433
Attn: AFAPL (APIE)   1

DISTRIBUTION (Cont'd)

Addressee	No. of Copies
Headquarters, United States Air Force Office of Scientific Research Washington, D. C. 2052	1
United States Army Research Office (Durham) Boc CM Duke Station Durham, North Carolina Attn: Dr. P. Kosting	1
McDonnell Aircraft Corporation Box 516 St. Louis 66, Missouri Attn: Dr. W. Van Camp	1
Thermo-Mechanics Res. Lab. Wright-Patterson AFB, Ohio 45433-DAR, USAF	1
NASA - Goddard Space Flight Center Library Greenbelt, Maryland, 20771	1
Electro-Optical Systems, Inc. 125 N. Vinedo Avenue Pasadena, California Attn: Dr. G. Cann	1
The Marquardt Corporation 16555 Saticoy Street Van Nuys, California Attn: Mr. Russell Page	1
Gianinni Scientific Corporation 3839 South Main Street Santa Ana, California Attn: Mr. Adriano Ducati	1

Addressee	No. of Copies
Thrust Systems Company 1641 Monrovia Costs/Mova, California Attn: W. Stoner	1
NASA Marshall Space Flight Center Library Huntsville, Alabama 35812	1
NASA Marshall Space Flight Building 4488 Huntsville, Alabama Attn: Mr. Dan Gates (MS-T)	1
Aeronautical Systems Division Wright-Patterson AFB, Ohio Attn: ASRMPE, F.L. Hommedieu	1
NASA Lewis Research Center 21000 Brookpark Road Cleveland, Ohio 44135 Attn: Technology Utilization Office	1
Philco Corporation Newport Beach, California Attn: R. Spongberg ATC	1
The Aerospace Corporation P. O. Box 95085 Los Angeles 45, California Library Technical Documents Group	1
Ling-Temco-Vought, Inc. Advanced Systems, Astro. Div. Box 6267 Dallas 22, Texas Attn: F. T. Esenwein	1

DISTRIBUTION (Concl'd)

Addressee	No. of Copies
NASA Lewis Research Center Spacecraft Technology Div. (MS 21-5) 2p000 Brookpark Road Cleveland, Ohio 44135 Attn: J. H. Childs	1
Northrop Corporation 3901 West Broadway Hawthorne, California Attn: Dr. E. B. Mikus	1
Materials Research Corp. Orangeburg, N.Y. 19062 Attn: Mr. Vernon E. Adler	1
Marguardt Corporation 16555 Saticoy Street Van Nuys, California Attn: Mr. Russell Page	1
Central Files	1
Research Library (+ 1 reproducible)	31